A domain-independent interaction integral for magneto-electro-elastic materials

Hongjun Yu, Linzhi Wu, Hui Li

PII: S0020-7683(13)00394-6
DOI: http://dx.doi.org/10.1016/j.ijsolstr.2013.10.005
Reference: SAS 8138

To appear in: *International Journal of Solids and Structures*

Received Date: 7 November 2012

Please cite this article as: Yu, H., Wu, L., Li, H., A domain-independent interaction integral for magneto-electro-elastic materials, *International Journal of Solids and Structures* (2013), doi: http://dx.doi.org/10.1016/j.ijsolstr.2013.10.005

A domain-independent interaction integral for magneto-electro-elastic materials

Hongjun Yu[1, 2 *], Linzhi Wu[1], Hui Li[2]

[1] Institute of Applied Mathematics, Harbin Institute of Technology, Harbin 150001, China

[2] School of Civil Engineering, Harbin Institute of Technology, Harbin, 150090, China

Abstract

Magneto-electro-elastic (MEE) materials usually consist of piezoelectric (PE) and piezomagnetic (PM) phases. Between different constituent phases, there exist lots of interfaces with discontinuous MEE properties. Complex interface distribution brings a great difficulty to the fracture analysis of MEE materials since the present fracture mechanics methods can hardly solve the fracture parameters efficiently of a crack surrounded by complex interfaces. This paper develops a new domain formulation of the interaction integral for the computation of the fracture parameters including stress intensity factors (SIFs), electric displacement intensity factor (EDIF) and magnetic induction intensity factor (MIIF) for linear MEE materials. The formulation derived here does not involve any derivatives of material properties and moreover, it can be proved that an arbitrary interface in the integral domain does not affect the validity and the value of the interaction integral. Namely, the interaction integral is domain-independent for material interfaces and thus, its application does not require material parameters to be continuous. Due to this advantage, the interaction integral becomes an effective approach for extracting the fracture parameters of MEE materials with complex interfaces. Combined with the extended finite element method (XFEM), the interaction integral is employed to solve several

[*]Corresponding author. Tel: +86 451 86403725, fax: +86 451 86403725.

E-mail address: yuhongjun@hit.edu.cn (Hongjun Yu)

representative problems to verify its accuracy and domain-independence. Good results show the effectiveness of the present method in the fracture analysis of MEE materials with continuous and discontinuous properties. Finally, the particulate MEE composites composed of PE and PM phases are considered and four schemes of different property-homogenization level are proposed for comparing their effectiveness.

Keywords: magneto-electro-elastic (MEE); particulate; crack; interaction integral; domain-independent; stress intensity factor (SIF); electric displacement intensity factor (EDIF); magnetic induction intensity factor (MIIF); extended finite element method (XFEM)

1. Introduction

Magneto-electro-elastic (MEE) materials were first observed by Van Suchtelen (1972) and Van Run et al. (1974) who found that the ferrite-ferroelectric composites possessing both piezoelectric (PE) and piezomagnetic (PM) phases exhibited a magneto-electric coupling effect. Possessing the ability of converting mechanical, electric and magnetic energy, MEE materials have drawn significant interest in several engineering fields as a class of important functional materials, such as magnetic field probes, electronic packaging, hydrophones, medical ultrasonic imaging, actuators, waveguides, sensors, phase invertors, transducers (Wu and Huang, 2000; Ma et al., 2012). However, a great drawback of MEE materials is their inherent brittleness and low fracture toughness (Sladek et al., 2011). Generally, these materials may fail prematurely in service due to some defects such as cracks and holes, arising during the manufacturing process and subsequent handling. For this reason, it is of great important to understand the fracture feature of MEE materials.

On the theoretical side, Liu et al. (2001) studied Green's functions for MEE materials involving a crack. Based on the extended Stroh formalism, Wang and Mai (2003) obtained a general two-dimensional (2D) solution of the MEE field around the crack tip. Gao et al. (2003, 2004) obtained the explicit solutions in closed forms for a crack in MEE solids. Song and Sih (2003) examined the crack initiation and growth behavior in a MEE body. Subsequently, considerable research work was carried out on the static and dynamic fracture problems of MEE materials (Wang and Mai, 2004, 2007; Chen et al., 2004; Li, 2005; Hu and Li, 2005; Yong and Zhou, 2007; Guo and Lu, 2010; Zhang, 2011; Zhong, 2011; Ma et al., 2012). MEE materials usually contain PE and PM phases and the interfaces between constituent phases may reduce the reliability of MEE materials since the interfaces generally act as sources of failures in service. In order to improve the reliability, researchers proposed the concept of functionally graded materials (FGMs), a category of non-homogeneous materials with properties varying continuously, and recently, the concept of FGMs is extended to MEE materials, called functionally graded MEE (FGMEE) materials. The cracks in a FGMEE solid subjected to anti-plane shear loading were first considered by Zhou and Wang (2004, 2006) using the Schmidt method. The fracture analyses of FGMEE materials are mostly restricted to a relatively simple anti-plane problems (Feng and Su, 2006; Ma et al., 2007, 2009; Li and Lee, 2008; Lee and Ma, 2010; Rangelov et al., 2011). Up to recent years, there are few research papers (Zhou and Chen, 2008; Ma and Lee, 2009; Rekik et al., 2012; Zhong and Lee, 2012) on the in-plane fracture problems of FGMEE materials.

Theoretical studies are mostly under some rigorous assumptions and thus, lots of

actual problems need to be solved by using numerical methods. On the numerical side, except the finite element method (FEM) (Rao and Kuna, 2008b), the boundary element method (BEM), the Meshless local Petrov-Galerkin (MLPG) method and the extended finite element method (XFEM) are mostly used to analyze the fracture problems of homogeneous MEE and FGMEE materials. Garcia-Sanchez et al. (2007), Dong et al. (2008), Rojas-Diaz et al. (2012) and Pasternak (2012) adopted the BEM to investigate the static crack problems of MEE materials. Rojas-Diaz et al. (2010) and Wunsche et al. (2012) employed the BEM to study fracture problems of MEE materials under dynamic loading. Sladek et al. (2008) and Li et al. (2009) applied the MLPG method to analyze a crack in homogeneous MEE media. Sladek et al. (2010, 2011) extended the MLPG method to examine crack problems of FGMEE materials subjected to the stationary and transient thermal and mechanical loading. Rojas-Diaz et al. (2011) and Bhargava et al. (2012) used the XFEM in static fracture and quasi-static crack propagation analyses of MEE solids.

The intensity factors (IFs) including stress intensity factors (SIFs), electric displacement intensity factor (EDIF) and magnetic induction intensity factor (MIIF) are the key fracture parameters charactering the crack-tip fields of linear MEE materials. As a powerful tool solving the fracture parameters, conservation integrals such as the J-integral, the J_i-integral and the M-integral are widely used to study the crack behaviors in pure elastic media in the past decades. Recently, these conservation integrals have also been developed to deal with MEE materials. Wang and Mai (2003) first derived a path-independent J-integral for homogeneous MEE materials. Tian and

Rajapakse (2005) discussed the J_i-integral and M-integral for a single crack and multi-crack problems in MEE media. For dynamic fracture problems of MEE solids, Chen (2009) established a dynamic contour integral which is equivalent to the dynamic energy release rate. He pointed out that the dynamic contour integral is path-independent for steady-state crack propagation in the absence of mechanical body force, thermal effect and electricity conduction. In order to decouple mode I and mode II SIFs in mixed-mode fracture, Stern et al. (1976) proposed the interaction integral for pure elastic solids on the basis of the J-integral by considering two admissible states. Enderlein et al. (2005) developed the interaction integral to study the fracture problems of homogeneous PE materials. Soon later, Rao and Kuna (2008a, b) exploited the interaction integral method for solving the IFs of functionally graded PE and FGMEE media. Due to the convenience in the post-processing of most numerical implementations, such as in FEM and XFEM, the domain form of an integral is generally adopted to replace the contour form. By selecting three types of the auxiliary fields for non-homogenous MEE materials, Rao and Kuna (2008b) gave three corresponding domain formulations of the interaction integral and discussed their precision differences. Recently, the domain form of the interaction integral is widely used in the static crack and quasi-static crack propagation analyses of MEE materials (Rojas-Diaz et al., 2011; Bhargava and Sharma, 2012).

To the best knowledge of the authors, almost all the previous fracture studies are focused on the MEE materials with continuous and differentiable properties and correspondingly, all the interaction integral published previously require material

properties to be differentiable. However, most of the MEE materials are typical composites composed of PE and PM phases and therefore, there exist unavoidably material interfaces between different phases. In addition, FGMEE materials actually are at least two-phase particulate composites synthesized in such a way that the volume fractions of the constituent materials vary continuously along a spatial direction to give a predetermined composition profile resulting in a relatively smooth variation of the mechanical properties (Rekik et al., 2012). Experimental studies (Cannillo et al., 2006) show that the microstructure and the interfaces between the constituents affect the fracture behaviors of FGMs obviously and therefore, as the research scale decreases down to a certain level, the interfaces in FGMs have to be considered. In order to analyze MEE materials with complex interfaces effectively, this paper aims to establish a fracture mechanics method which is not require material properties to be continuous and differentiable.

In the previous studies on pure elastic and PE media (Yu et al., 2009, 2010a, b, 2012), the authors have established an interaction integral which is domain-independent for material interfaces. In this paper, the authors will attempt to establish a domain-independent interaction integral for MEE media. Our contributions can be stressed as follows. 1) The interaction integral derived here is domain-independent for material interfaces. Therefore, the present interaction integral method may become an extremely promising technique in the fracture analysis of MEE materials with complex interfaces. 2) The expression of the present interaction integral does not contain any derivatives of MEE properties, which gets rid of the requirement on the differentiability

of material properties and thus, facilitates the practical implementation of numerical computations since the derivatives of actual material properties are usually extremely difficult to acquire.

The outline of this paper is as follows. Section 2 reviews the basic equations of MEE materials briefly and introduces an expanded tensor notation to simplify their expressions. Section 3 gives the definitions of the interaction integral and the auxiliary fields for MEE media, and provides the relation between the interaction integral and the IFs. Section 4 derives a new domain form of the interaction integral for MEE media with continuous properties. Section 5 derives the domain form of the interaction integral for MEE media with discontinuous properties and gives the rigorous proof that an arbitrary interface in the integral domain does not affect the value of the interaction integral. Section 6 describes the extended finite element method (XFEM) briefly and provides the discretization of the interaction integral. Section 7 presents several numerical examples. Finally, Section 8 gives a summary and some conclusions.

2. Basic relations for MEE media

For MEE media, the governing equations and the boundary conditions are given first. Then, we will define the expanded tensors by which the expressions of the basic equations will be simplified.

2.1 Governing equations

The field equations for a linear MEE medium subjected to magneto-electro-mechanical loads in the absence of body forces, concentrated electric charges and concentrated magnetic source are:

- Constitutive equations:

$$\begin{aligned} \sigma_{ij} &= C_{ijkl}\varepsilon_{kl} - e_{lij}E_l - h_{lij}H_l \\ D_i &= e_{ikl}\varepsilon_{kl} + \kappa_{il}E_l + \beta_{il}H_l \\ B_i &= h_{ikl}\varepsilon_{kl} + \beta_{il}E_l + \gamma_{il}H_l \end{aligned} \tag{1}$$

The constitutive equations can also be expressed as

$$\begin{aligned} \varepsilon_{ij} &= S_{ijkl}\sigma_{kl} + d_{lij}D_l + g_{lij}B_l \\ E_i &= -d_{ikl}\sigma_{kl} + \mu_{il}D_l + \alpha_{il}B_l \\ H_i &= -g_{ikl}\sigma_{kl} + \alpha_{il}D_l + \lambda_{il}B_l \end{aligned} \tag{2}$$

- Kinematic equations:

$$\varepsilon_{ij} = \frac{1}{2}(u_{i,j} + u_{j,i}), \quad E_i = -\phi_{,i}, \quad H_i = -\varphi_{,i} \tag{3}$$

- Equilibrium equations:

$$\sigma_{ij,j} = 0, \quad D_{i,i} = 0, \quad B_{i,i} = 0 \tag{4}$$

where the variables marked by the subscripts i, j, k and l $(i, j, k, l = 1, 2, 3)$ are the components of a vector or a tensor; u_i, σ_{ij} and ε_{ij} are the elastic displacement, stress, strain tensors, respectively; ϕ, D_i and E_i are the electric potential, electric displacement, electric field tensors, respectively; φ, B_i and H_i are magnetic potential, magnetic induction, magnetic field tensors, respectively; C_{ijkl}, S_{ijkl}, κ_{il}, μ_{il}, γ_{il} and λ_{il} are the elastic stiffness, elastic compliance, dielectric permittivity, dielectric impermeability, magnetic permeability and reluctivity tensors, respectively; e_{ikl}, d_{ikl}, h_{ikl}, g_{ikl}, β_{il} and α_{il} are the PE stress, PE strain, PM stress, PM strain, electro-magnetic and magneto-electric tensors, respectively. A comma denotes partial differentiation and the repetition of an index (i, j, k, l and I, J, K, L) implies summation with respect to the index over its range.

2.2 Boundary conditions

Consider a MEE medium occupying the space Ω enclosed by surface Λ. The boundary surface $\Lambda = \Lambda_\sigma + \Lambda_u = \Lambda_D + \Lambda_\phi = \Lambda_B + \Lambda_\varphi$ On the boundaries Λ_σ, Λ_D and Λ_B, the resultants of the stresses, electric displacements and magnetic inductions are respectively

$$\begin{aligned} &\sigma_{ij} n_i = t_j^0, \quad \text{on } \Lambda_\sigma \\ &D_i n_i = -\omega^0, \quad \text{on } \Lambda_D \\ &B_i n_i = -\tilde{\omega}^0, \quad \text{on } \Lambda_B \end{aligned} \tag{5}$$

where t_j^0, ω^0 and $\tilde{\omega}^0$ are prescribed values on Λ_σ, Λ_D and Λ_B, respectively, and n_i is the outward unit normal vector to Λ. On the boundaries Λ_u, Λ_ϕ and Λ_φ, the displacements, electric potential and magnetic potential are, respectively

$$\begin{aligned} &u_i = u_i^0, \quad \text{on } \Lambda_u \\ &\phi = \phi^0, \quad \text{on } \Lambda_\phi \\ &\varphi = \varphi^0, \quad \text{on } \Lambda_\varphi \end{aligned} \tag{6}$$

where u_i^0, ϕ^0 and φ^0 are prescribed values on Λ_u, Λ_ϕ and Λ_φ, respectively.

2.3 Expanded tensor notation

By letting

$$\begin{aligned} &u_4 = \phi, \quad u_5 = \varphi, \\ &\sigma_{4j} = D_j, \quad \sigma_{5j} = B_j, \quad \sigma_{i'j'} = 0, \\ &2\varepsilon_{4j} = -E_j, \quad 2\varepsilon_{5j} = -H_j, \quad \varepsilon_{i'j'} = 0 \end{aligned} \tag{7}$$

where $i, j, k, l = 1, 2, 3$ and $i', j', k', l' = 4, 5$, and letting

$$\begin{aligned} &C_{4jkl} = e_{jkl}, \quad C_{5jkl} = h_{jkl}, \\ &C_{4j4l} = -\kappa_{jl}, \quad C_{5j5l} = -\gamma_{jl}, \quad C_{4j5l} = -\beta_{jl}, \\ &C_{i'j'kl} = C_{i'j'k'l} = 0, \quad C_{i'j'k'l'} \text{ arbitrary value} \\ &2S_{4jkl} = d_{jkl}, \quad 2S_{5jkl} = g_{jkl}, \\ &4S_{4j4l} = -\mu_{jl}, \quad 4S_{5j5l} = -\lambda_{jl}, \quad 4S_{4j5l} = -\alpha_{jl}, \\ &S_{i'j'kl} = S_{i'j'k'l} = 0, \quad S_{i'j'k'l'} \text{ determined by } C_{i'j'k'l'} \end{aligned} \tag{8}$$

we can extend the tensors u_i, σ_{ij}, ε_{ij}, C_{ijkl} and S_{ijkl} respectively into the expanded

tensors u_I, σ_{IJ}, ε_{IJ}, C_{IJKL} and S_{IJKL} $(I,J,K,L=1-5)$ which have the following symmetry properties

$$\begin{aligned} &\sigma_{IJ}=\sigma_{JI}, \quad \varepsilon_{IJ}=\varepsilon_{JI}, \\ &C_{IJKL}=C_{JIKL}=C_{IJLK}=C_{KLIJ}, \\ &S_{IJKL}=S_{JIKL}=S_{IJLK}=S_{KLIJ} \end{aligned} \tag{9}$$

Here, the expanded compliance tensor S_{IJKL} and the expanded stiffness tensor C_{IJKL} meet the relation $C_{IJST}S_{STKL}=\delta_{IK}\delta_{JL}$, where the symbol δ_{IK} is Kronecker delta.

Since an actual coordinate system does not contain the coordinate components x_4 and x_5, the components of the unit vector n_j in x_4 and x_5 directions can be defined as zero and the derivatives of a variable with respect to x_4 and x_5 can also be defined as zero, i.e.,

$$n_4=n_5=0, \quad (*)_{,4}=(*)_{,5}=0 \tag{10}$$

where $(*)$ denotes an arbitrary variable.

On the basis of the above definitions, the governing Eqs. (1)-(4) can be expressed in an expanded tensor notation respectively as

$$\sigma_{IJ}=C_{IJKL}\varepsilon_{KL} \tag{11}$$

$$\varepsilon_{IJ}=S_{IJKL}\sigma_{KL} \tag{12}$$

$$\varepsilon_{IJ}=\frac{1}{2}(u_{I,J}+u_{J,I}) \tag{13}$$

$$\sigma_{IJ,J}=0 \tag{14}$$

And the boundary conditions in Eqs. (5) and (6) can be expressed respectively as

$$\sigma_{IJ}n_I=t_J^0, \quad \text{on } \Lambda_\sigma, \Lambda_D \text{ and } \Lambda_B \tag{15}$$

$$u_I=u_I^0, \quad \text{on } \Lambda_u, \Lambda_\phi \text{ and } \Lambda_\varphi \tag{16}$$

3. Definition of the interaction integral

The interaction integral is derived from the J-integral by superimposing two admissible states, i.e., an actual state and an auxiliary state. Selecting a suitable auxiliary state is a key step to establish a domain-independent interaction integral. Therefore, in this section, the auxiliary fields will be given first. Then, the definition of the interaction integral will be described. Finally, the relation between the interaction integral and the IFs will be introduced.

3.1 Auxiliary fields

For non-homogeneous MEE materials, the auxiliary fields have three alternative choices (Rao and Kuna, 2008b). Here, an incompatibility formulation is selected. As shown in Fig. 1, the detailed auxiliary fields are defined in the polar coordinate system (r,θ) with the origin at the crack tip. The expanded auxiliary displacements u_J^{aux} and auxiliary stresses σ_{IJ}^{aux} are defined as

$$u_J^{aux}(r,\theta)=\sqrt{\frac{2r}{\pi}}\sum_N K_N^{aux} f_J^N(\theta) \tag{17}$$

$$\sigma_{IJ}^{aux}(r,\theta)=\frac{1}{\sqrt{2\pi r}}\sum_N K_N^{aux} g_{IJ}^N(\theta) \tag{18}$$

where the summation over $N=\{II,\ I,\ III,\ D,\ B\}$ comprises the fracture opening modes; K_I^{aux}, K_{II}^{aux}, K_{III}^{aux}, K_D^{aux} and K_B^{aux} denote the auxiliary mode-I, mode-II, mode-III mechanical SIFs, EDIF and MIIF, respectively. The angular functions $f_J^N(\theta)$ and $g_{IJ}^N(\theta)$ are the standard angular functions for a crack in a homogeneous MEE medium, which depend only on the material properties at the crack-tip location. The detailed definitions of the angular functions can be found in the appendix.

The expanded auxiliary strains are defined as

$$\varepsilon_{IJ}^{aux} = S_{IJKL}(\mathbf{x})\sigma_{KL}^{aux} \tag{19}$$

It can be found that the constitutive equations of the auxiliary fields use the same material constants as those of the actual fields. The expanded auxiliary stresses satisfy equilibrium equations in the absence of body forces, concentrated electric charges and concentrated magnetic source, i.e.,

$$\sigma_{IJ,J}^{aux} = 0\,. \tag{20}$$

However, the above definition of the auxiliary strains leads to that in general,

$$\varepsilon_{IJ}^{aux} \neq \frac{1}{2}(u_{I,J}^{aux} + u_{J,I}^{aux}), \tag{21}$$

while another strain tensor defined by

$$\varepsilon_{IJ}^{aux0} = S_{IJKL}^{tip}\sigma_{KL}^{aux} \tag{22}$$

satisfies the relation

$$\varepsilon_{IJ}^{aux0} = \frac{1}{2}(u_{I,J}^{aux} + u_{J,I}^{aux}) \tag{23}$$

where S_{IJKL}^{tip} is the expanded compliance tensor at the crack-tip location. It needs to be pointed out that the auxiliary strain tensor used in the interaction integral is ε_{IJ}^{aux}, not ε_{IJ}^{aux0}.

3.2 Interaction integral

As shown in Fig. 1, for a 2D cracked MEE body, the J-integral (Wang and Mai, 2003) is

$$J = \lim_{\Gamma_\varepsilon \to 0} \int_{\Gamma_\varepsilon} (F\delta_{1j} - \sigma_{ij}u_{i,1} - D_j\phi_{,1} - B_j\varphi_{,1})n_j d\Gamma \tag{24}$$

where F is the electro-magnetic enthalpy density; n_j is the unit outward normal vector to the contour Γ_ε. For linear MEE media, $F = (\sigma_{ij}\varepsilon_{ij} - D_iE_i - B_iH_i)/2$ and according to Section 2.3, it can be expressed in an expanded tensor notation as

$F = \sigma_{IJ}\varepsilon_{IJ}/2$. Similarly, the J-integral can also be expressed as

$$J = \lim_{\Gamma_\varepsilon \to 0} \int_{\Gamma_\varepsilon} (\frac{1}{2}\sigma_{IK}\varepsilon_{IK}\delta_{1J} - \sigma_{IJ}u_{I,1})n_J d\Gamma \tag{25}$$

Superposition of the actual fields (u_I, σ_{IJ}, ε_{IJ}) and the auxiliary fields (u_I^{aux}, σ_{IJ}^{aux}, ε_{IJ}^{aux}) leads to another equilibrium state (state S) for which the J-integral is

$$J^{(S)} = \lim_{\Gamma_\varepsilon \to 0} \int_{\Gamma_\varepsilon} \begin{bmatrix} \frac{1}{2}(\sigma_{IK} + \sigma_{IK}^{aux})(\varepsilon_{IK} + \varepsilon_{IK}^{aux})\delta_{1J} \\ -(\sigma_{IJ} + \sigma_{IJ}^{aux})(u_{I,1} + u_{I,1}^{aux}) \end{bmatrix} n_J d\Gamma \tag{26}$$

By expanding Eq. (26), it can be obtained that

$$J^{(S)} = J + J^{aux} + I \tag{27}$$

Here, J is the J-integral aroused by the actual fields alone,

$$J^{aux} = \lim_{\Gamma_\varepsilon \to 0} \int_{\Gamma_\varepsilon} (\frac{1}{2}\sigma_{IK}^{aux}\varepsilon_{IK}^{aux}\delta_{1J} - \sigma_{IJ}^{aux}u_{I,1}^{aux})n_J d\Gamma \tag{28}$$

is the J-integral aroused by the auxiliary fields alone and

$$I = \lim_{\Gamma_\varepsilon \to 0} \int_{\Gamma_\varepsilon} \begin{bmatrix} \frac{1}{2}(\sigma_{IK}\varepsilon_{IK}^{aux} + \sigma_{IK}^{aux}\varepsilon_{IK})\delta_{1J} \\ -\sigma_{IJ}u_{I,1}^{aux} - \sigma_{IJ}^{aux}u_{I,1} \end{bmatrix} n_J d\Gamma \tag{29}$$

is the interaction integral. According to the definition of the auxiliary strains in Eq. (19), it can be observed that $\sigma_{IK}\varepsilon_{IK}^{aux} = \sigma_{IK}^{aux}\varepsilon_{IK}$ and hence, I can be simplified as

$$I = \lim_{\Gamma_\varepsilon \to 0} \int_{\Gamma_\varepsilon} (\sigma_{IK}^{aux}\varepsilon_{IK}\delta_{1J} - \sigma_{IJ}u_{I,1}^{aux} - \sigma_{IJ}^{aux}u_{I,1})n_J d\Gamma \tag{30}$$

3.3 Extraction of the IFs from the interaction integral

For linear MEE solids, the J-integral is equal to the total potential energy release rate and thus, the J-integral can be expressed as (Rao and Kuna, 2008b)

$$J = \frac{1}{2}\mathbf{K}^T\mathbf{Y}\mathbf{K} \tag{31}$$

where $\mathbf{K} = [K_{II},\ K_I,\ K_{III},\ K_D,\ K_B]^T$ is the vector of the five IFs. $\mathbf{Y}$ is the (5×5) generalized Irwin matrix which depends on the material constants at the

crack-tip location and its definition is given in the appendix.

The J-integral for the superposition of the two fields (state S) can be written as

$$J^{(S)} = \frac{1}{2}(\mathbf{K}+\mathbf{K}^{aux})^T \mathbf{Y}(\mathbf{K}+\mathbf{K}^{aux}) \tag{32}$$

where $\mathbf{K}^{aux} = [K_{II}^{aux},\ K_I^{aux},\ K_{III}^{aux},\ K_D^{aux},\ K_B^{aux}]^T$ is the vector of the auxiliary IFs. Similarly to Eq. (27), $J^{(S)}$ can also be expanded as J, J^{aux} and I. Due to the symmetry of the matrix $\mathbf{Y}$, the interaction integral can be expressed as

$$I = \mathbf{K}^T \mathbf{Y} \mathbf{K}^{aux} \tag{33}$$

For 2D case, $K_{III} = K_{III}^{aux} = 0$. If the auxiliary fields are chosen to be the state corresponding to the fracture opening mode II, namely, $K_{II}^{aux} = 1$, $K_I^{aux} = K_D^{aux} = K_B^{aux} = 0$, Eq. (33) reduces to

$$I^{(II)} = K_{II}Y_{11} + K_I Y_{12} + K_D Y_{14} + K_B Y_{15} \tag{34}$$

By letting $K_I^{aux} = 1$, $K_{II}^{aux} = K_D^{aux} = K_B^{aux} = 0$, Eq. (33) reduces to

$$I^{(I)} = K_{II}Y_{21} + K_I Y_{22} + K_D Y_{24} + K_B Y_{25} \tag{35}$$

By letting $K_D^{aux} = 1$, $K_I^{aux} = K_{II}^{aux} = K_B^{aux} = 0$, Eq. (33) reduces to

$$I^{(D)} = K_{II}Y_{41} + K_I Y_{42} + K_D Y_{44} + K_B Y_{45} \tag{36}$$

By letting $K_B^{aux} = 1$, $K_I^{aux} = K_{II}^{aux} = K_D^{aux} = 0$, Eq. (33) reduces to

$$I^{(B)} = K_{II}Y_{51} + K_I Y_{52} + K_D Y_{54} + K_B Y_{55} \tag{37}$$

If $I^{(II)}$, $I^{(I)}$, $I^{(D)}$ and $I^{(B)}$ are known, by simultaneously solving Eqs. (34)-(37), the IFs K_I, K_{II}, K_D and K_B can be obtained . Next, how to calculate the values of the interaction integral will be discussed.

4. Interaction integral for MEE media with continuous properties

The infinitesimal contour integral in Eq. (30) can not be obtained directly in

numerical calculations and thus, it is usually converted into an equivalent domain integral which can avoid the potential source of inaccuracy in the computation process of a line integral (Moran and Shih, 1987). In this section, we will discuss the interaction integral for a 2D MEE solid with material properties varying continuously and derive a new domain formulation different from that given by Rao and Kuna (2008b).

4.1 An equivalent closed contour form of the interaction integral

To begin, as shown in Fig. 1, consider two domain A and A_0 enclosed respectively by the contours Γ_B and Γ_0, where $\Gamma_0 = \Gamma_B + \Gamma_\varepsilon^- + \Gamma_c^+ + \Gamma_c^-$ and Γ_ε^- is the opposite path of the contour Γ_ε. Therefore, taking the limit $\Gamma_\varepsilon \to 0$ leads to $A_0 \to A$. Next, we define an integral on the closed contour Γ_0 as

$$\overline{I} = \lim_{\Gamma_\varepsilon \to 0} \oint_{\Gamma_0} P_{1J} n_J q d\Gamma \tag{38}$$

where the expression of P_{1J} is identical with that in the bracket in Eq. (30), i.e.,

$$P_{1J} = \sigma_{IK}^{aux} \varepsilon_{IK} \delta_{1J} - \sigma_{IJ} u_{I,1}^{aux} - \sigma_{IJ}^{aux} u_{I,1} \tag{39}$$

Here, P_{1J} can be regarded as the mutual MEE energy momentum tensor in the spirit of Eshelby's concept; q is an arbitrary weight function with value varying smoothly from 1 on Γ_ε to 0 on Γ_B.

In this paper, the crack faces Γ_c^+ and Γ_c^- are assumed to be mechanical traction-free ($\sigma_{ij} n_j = 0$), electrically impermeable ($D_j n_j = 0$) and magnetically impermeable ($B_j n_j = 0$), and according to Section 2.3, it can be called the expended traction-free condition expressed by

$$\sigma_{IJ} n_J = 0, \quad \text{on } \Gamma_c^+ \text{ and } \Gamma_c^- \tag{40}$$

According to Eqs. (17)-(19), it can be noted that the auxiliary fields also meet the

expended traction-free condition expressed by

$$\sigma_{IJ}^{aux} n_J = 0, \quad \text{on } \Gamma_c^+ \text{ and } \Gamma_c^- \tag{41}$$

According to the relations that $q = 0$ on Γ_B, $\sigma_{IJ} n_J = 0$, $\sigma_{IJ}^{aux} n_J = 0$ and $n_1 = 0$ on Γ_c^+ and Γ_c^-, it can be easily proved that

$$I = -\overline{I} = -\lim_{\Gamma_\varepsilon \to 0} \oint_{\Gamma_0} P_{1J} n_J q d\Gamma \tag{42}$$

4.2 Domain formulation of the interaction integral

Applying divergence theorem to Eq. (42), one obtains

$$I = -\int_A (P_{1J} q_{,J} + P_{1J,J} q) dA \tag{43}$$

Substituting Eqs. (13), (14) and (20) into $P_{1J,J}$, one obtains

$$P_{1J,J} = \sigma_{IJ,1}^{aux} \varepsilon_{IJ} - \sigma_{IJ} u_{I,J1}^{aux} \tag{44}$$

Substituting Eqs. (12), (22) and (23) into Eq. (44), we have

$$P_{1J,J} = \sigma_{IJ,1}^{aux} [S_{IJKL}(\mathbf{x}) - S_{IJKL}^{tip}] \sigma_{KL} \tag{45}$$

By substituting the expressions P_{1J} (Eq. (39)) and $P_{1J,J}$ (Eq. (45)) into Eq. (43), the domain formulation of the interaction integral is finally simplified as

$$\begin{aligned} I = & \int_A (\sigma_{IJ} u_{I,1}^{aux} + \sigma_{IJ}^{aux} u_{I,1} - \sigma_{IK}^{aux} \varepsilon_{IK} \delta_{1J}) q_{,J} dA \\ & + \int_A \sigma_{IJ,1}^{aux} [S_{IJKL}^{tip} - S_{IJKL}(\mathbf{x})] \sigma_{KL} q dA \end{aligned} \tag{46}$$

Since only the material properties at the crack-tip location are adopted in the expanded auxiliary stresses and displacements, there are no derivatives of material properties in the formulation of the interaction integral given in Eq. (46). This advantage may bring a great convenience to the application of the present interaction integral, since it is usually very difficult to obtain the derivatives of material properties in many actual cases. Moreover, no derivatives of material properties in Eq. (46) imply

that the present interaction integral does not require the material properties of MEE media to be differentiable.

5. Interaction integral for MEE media with discontinuous properties

In the previous section, it has been shown that the interaction integral does not require material properties to be differentiable. However, the material properties are still required to be continuous. In this section, we will discuss whether this continuity condition of material properties is necessary.

5.1 Interaction integral for a MEE solid with an interface

As shown in Fig. 2, in domain A, there is a perfectly bonded interface $\Gamma_{\text{interface}}$ on which all material parameters are discontinuous. Due to the existence of the interface $\Gamma_{\text{interface}}$, the domain A is divided into two sub-domains A_1 and A_2 enclosed respectively by the closed contours Γ_{01} and Γ_{02}. As a result, $A = A_1 + A_2$, $\Gamma_{01} = \Gamma_{B1} + \Gamma_{\text{interface}} + \Gamma_{B3} + \Gamma_c^+ + \Gamma_\varepsilon^- + \Gamma_c^-$ and $\Gamma_{02} = \Gamma_{B2} + \Gamma_{\text{interface}}^-$, where $\Gamma_{\text{interface}}^-$ is the opposite path of $\Gamma_{\text{interface}}$. In order to apply divergence theorem, the interaction integral needs to be expressed as

$$I = -\lim_{\Gamma_\varepsilon \to 0} \oint_{\Gamma_{01}} P_{1J} n_J q d\Gamma - \oint_{\Gamma_{02}} P_{1J} n_J q d\Gamma + I^*_{\text{interface}} \tag{47}$$

where $I^*_{\text{interface}}$ is a line integral along the interface with the expression as

$$\begin{aligned} I^*_{\text{interface}} &= \int_{\Gamma_{\text{interface}}} P_{1J}^{①} n_J q d\Gamma + \int_{\Gamma_{\text{interface}}^-} P_{1J}^{②} n_J q d\Gamma \\ &= \int_{\Gamma_{\text{interface}}} (P_{1J}^{①} - P_{1J}^{②}) n_J q d\Gamma \end{aligned} \tag{48}$$

Here, the variables or expressions marked by the superscripts ① and ② means that they belong to the domains A_1 and A_2, respectively. Applying divergence theorem to the first and second integrals in Eq. (47), respectively, we have

$$I = -\int_A (P_{1J} q_{,J} + P_{1J,J} q) dA + I^*_{\text{interface}} \tag{49}$$

The value of the interface integral $I^*_{\text{interface}}$ will be discussed in the following.

5.2 Interface integral $I^*_{\text{interface}}$

According to the definitions of the auxiliary fields, the expanded auxiliary stresses, displacements and their derivatives are continuous on the interface. Therefore, there are the relations $(\partial u_I^{aux}/\partial x_1)^{①} = (\partial u_I^{aux}/\partial x_1)^{②} = \partial u_I^{aux}/\partial x_1$ and $(\sigma_{IJ}^{aux})^{①} = (\sigma_{IJ}^{aux})^{②} = \sigma_{IJ}^{aux}$, and applying these conditions, we can simplify the interface integral $I^*_{\text{interface}}$ in Eq. (48) as

$$I^*_{\text{interface}} = \int_{\Gamma_{\text{interface}}} \begin{Bmatrix} \sigma_{IJ}^{aux}(\varepsilon_{IJ}^{①} - \varepsilon_{IJ}^{②}) n_1 - n_I(\sigma_{IJ}^{①} - \sigma_{IJ}^{②}) \dfrac{\partial u_J^{aux}}{\partial x_1} \\ -n_I \sigma_{IJ}^{aux}[(\dfrac{\partial u_J}{\partial x_1})^{①} - (\dfrac{\partial u_J}{\partial x_1})^{②}] \end{Bmatrix} q d\Gamma \tag{50}$$

Since the interface is in equilibrium, the resultant on the interface is zero. Namely,

$$n_I \sigma_{IJ}^{①} = n_I \sigma_{IJ}^{②} \tag{51}$$

According to the perfectly bonded assumption of the interface, the derivatives of the expanded displacements with respect to the curve $\Gamma_{\text{interface}}$ should be equal on both sides of the interface. If we define the curvilinear coordinates of a point p as

$$\eta_1 = \sqrt{(x_1 - x_{10})^2 + (x_2 - x_{20})^2}, \quad \eta_2 = \int_0^{p_0} d\Gamma \tag{52}$$

where $p_0(x_{10}, x_{20})$ is the point on $\Gamma_{\text{interface}}$ closest to the point $p(x_1, x_2)$ as shown in Fig. 3, this continuity condition of the displacement derivatives can be expressed as

$$(\frac{\partial u_J}{\partial \eta_2})^{①} = (\frac{\partial u_J}{\partial \eta_2})^{②} \tag{53}$$

In order to simplify the first integrand in Eq. (50), applying the strain-displacement

relations of actual fields in Eq. (13), one obtains

$$\sigma_{IJ}^{aux}(\varepsilon_{IJ}^{①}-\varepsilon_{IJ}^{②})n_1=\sigma_{IJ}^{aux}[(\frac{\partial u_J}{\partial x_I})^{①}-(\frac{\partial u_J}{\partial x_I})^{②}]n_1 \tag{54}$$

It can be noted from Eq. (52) that $\partial\eta_1/\partial x_i=n_i$ and according to the definitions in Eq. (10), it can be expanded as $\partial\eta_1/\partial x_I=n_I$. Substituting the chain rule formulation $\partial u_J/\partial x_I=(\partial u_J/\partial\eta_K)(\partial\eta_K/\partial x_I)$, $\partial\eta_1/\partial x_I=n_I$, Eqs. (10) and (53) into Eq. (54), one can simplify the first integrand of the interface integral $I_{\text{interface}}^{*}$ as

$$\sigma_{IJ}^{aux}(\varepsilon_{IJ}^{①}-\varepsilon_{IJ}^{②})n_1=n_I\sigma_{IJ}^{aux}[(\frac{\partial u_J}{\partial\eta_1})^{①}-(\frac{\partial u_J}{\partial\eta_1})^{②}]n_1 \tag{55}$$

Using the relations $\partial u_J/\partial x_1=(\partial u_J/\partial\eta_K)(\partial\eta_K/\partial x_1)$, $\partial\eta_1/\partial x_1=n_1$ and Eq. (53), we can write the third integrand of the interface integral $I_{\text{interface}}^{*}$ as

$$n_I\sigma_{IJ}^{aux}[(\frac{\partial u_J}{\partial x_1})^{①}-(\frac{\partial u_J}{\partial x_1})^{②}]=n_I\sigma_{IJ}^{aux}[(\frac{\partial u_J}{\partial\eta_1})^{①}-(\frac{\partial u_J}{\partial\eta_1})^{②}]n_1 \tag{56}$$

Substituting Eqs. (51), (55) and (56) into Eq. (50) yields

$$I_{\text{interface}}^{*}=0 \tag{57}$$

The same result in Eq (57) can be obtained for the interface across the crack face.

5.3 Discussion on the interaction integral

Substituting Eq. (57) into Eq. (49), the same expression as Eq. (46) is obtained when the integral domain contains an arbitrary interface, which implies that Eq. (46) is still valid for MEE materials with discontinuous properties. Namely, the interaction integral method does not require material properties to be continuous and hence, it may become an extremely promising method for the fracture analysis of MEE materials with complex interfaces. Moreover, compared with the formulation in the papers published previously (Rao and Kuna, 2008b; Sladek et al., 2011), the expression in Eq. (46) can

facilitate the numerical implementation since the integral domain can be chosen as a regular area containing arbitrary interfaces.

If the crack faces in the integral domain A are curved as shown in Fig. 4, it can be derived that a line integral along the crack faces $I_{crackface}$ needs to be added into Eq. (46), namely, the expression of the interaction integral becomes

$$I = \int_A (\sigma_{IJ} u^{aux}_{I,1} + \sigma^{aux}_{IJ} u_{I,1} - \sigma^{aux}_{IK} \varepsilon_{IK} \delta_{1J}) q_{,J} dA + \int_A \sigma^{aux}_{IJ,1} [S^{tip}_{IJKL} - S_{IJKL}(\mathbf{x})] \sigma_{KL} q dA + I_{crackface} \tag{58}$$

where

$$I_{crackface} = \int_{\Gamma_c^+ + \Gamma_c^- + \Gamma_A^+ + \Gamma_A^-} P_{1J} n_J q d\Gamma \tag{59}$$

where Γ_A^+ and Γ_A^- are the fictitious crack faces tangent to the crack tip. Considering the boundary conditions $n_J \sigma_{IJ} = 0$ on Γ_c^+ and Γ_c^-, $n_J \sigma^{aux}_{IJ} = 0$ and $n_1 = 0$ on Γ_A^+ and Γ_A^-, Eq. (59) can be simplified as

$$I_{crackface} = \int_{\Gamma_c^+ + \Gamma_c^-} (\sigma^{aux}_{IJ} \varepsilon_{IJ} n_1 - n_J \sigma^{aux}_{IJ} u_{I,1}) q dA - \int_{\Gamma_A^+ + \Gamma_A^-} n_J \sigma_{IJ} u^{aux}_{I,1} q dA \tag{60}$$

This interaction integral formulation for MEE media is of the same form as that for pure elastic media (Yu et al., 2009) by extending the range of indices from 1-3 to 1-5.

6. Numerical implementation of the interaction integral

The interaction integral method is implemented in conjunction with the extended finite element method (XFEM) since the XFEM can greatly simplify the analysis of fracture problems, especially, crack propagation problems. Therefore, the XFEM is introduced briefly.

6.1 XFEM for MEE media

For a pure elastic medium, the XFEM was developed by Belytschko and Black (1999) and Moës et al. (1999) who introduced the local enrichment functions into standard displacement-based approximation to characterize the local features. Therefore, the XFEM allows discontinuous boundaries, such as cracks or material interfaces, to be independent of the mesh. Recently, the XFEM is extended to MEE media (Rojas-Diaz et al., 2011; Bhargava and Sharma, 2012). The approximations of the expanded displacements are adopted as

$$u_I^h(\mathbf{x}) = \sum_{P\in\Omega_0} N_P(\mathbf{x})\left[u_I^P + \psi(\mathbf{x})b_I^P + \bar{H}_P(\mathbf{x})c_I^P\right] \tag{61}$$

where, $N_P(\mathbf{x})$ is the standard finite element shape function, the enrichment function $\psi(\mathbf{x}) = R(\mathbf{x})\left|\mathbf{x}-\bar{\mathbf{x}}\right|$, where $R(\mathbf{x}) = \sum_{Q\in\Omega_1} N_Q(\mathbf{x})$ is a ramp function (Fries, 2008), and $\bar{H}_P(\mathbf{x}) = H(\mathbf{x}-\bar{\bar{\mathbf{x}}}) - H(\mathbf{x}_P-\bar{\bar{\mathbf{x}}})$ is the shifted Heaviside step function which is zero for the node $P\notin\Omega_2$; u_I^P is the nodal displacement, and b_I^P and c_I^P are the additional degrees of freedom. As shown in Fig. 5, $\mathbf{x}$, $\bar{\mathbf{x}}$, $\bar{\bar{\mathbf{x}}}$ and $\mathbf{x}_P$ denote a point at arbitrary position, on an interface, on a crack face and on node P, respectively; Ω_0, Ω_1 and Ω_2 are the set of all nodes in mesh, the set of the enriched nodes for an interface and the set of the enriched nodes for a crack, respectively.

6.2 Numerical discretization of the interaction integral

In order to compute the value of the interaction integral according to the displacements, stresses and strains obtained by the XFEM, Eq. (46) should be discretized as

$$I = \sum_{e=1}^{e_A}\sum_{p=1}^{p_e}\left\{\begin{bmatrix}(\sigma_{IJ}u_{I,1}^{aux} + \sigma_{IJ}^{aux}u_{I,1})q_{,J} - \sigma_{IJ}^{aux}\varepsilon_{IJ}q_{,1}\\ +\sigma_{IJ,1}^{aux}(S_{IJKL}^{tip} - S_{IJKL})\sigma_{KL}q\end{bmatrix}\left|\mathbf{J}\right|w\right\}_p \tag{62}$$

Here, e_A is the number of elements in the integral domain A; p_e is the number of integration points in one element; $|\mathbf{J}|$ represents the determinant of Jacobian matrix; w is the corresponding weight factor. Except S_{IJKL}^{tip}, all variables in Eq. (62) take values at the integration point p.

In this paper, the quadrature used by Yu et al. (2009) is adopted. In details, for the standard elements, 3×3 Gauss quadrature is used. For the elements cut by the crack, the separately integrating on each side of the crack is executed by using a decomposition of the elements into sub-triangles and four-point integration rule is used on each sub-triangle. For the elements containing interfaces, the follow integration strategy is adopted: each element is divided into 3×3 sub-domains and 3×3 Gauss quadrature is used in each sub-domain, which leads to that one of such elements contains 81 integration points. Meanwhile, actual properties at integration points are employed in the process of forming the element stiffness matrix.

7. Numerical examples and discussions

At first, several benchmark fracture problems of MEE materials are considered to verify the accuracy and the domain-independence of the interaction integral. Then, our attention will be focused on the crack problems of a particulate MEE plate composed of PE and PM phases.

For all examples in this paper, plain strain condition and magneto-electrically impermeable crack surface conditions are prescribed. Using the relation between the indices $11\rightarrow1$, $22\rightarrow2$, $33\rightarrow3$, $23\rightarrow4$, $31\rightarrow5$, $12\rightarrow6$, the constitutive Eq. (1) can be written in Voigt notation as:

$$\begin{aligned} \sigma_\alpha &= C_{\alpha\beta}\varepsilon_\beta - e_{i\alpha}E_i - h_{i\alpha}H_i \\ D_i &= e_{i\beta}\varepsilon_\beta + \kappa_{ij}E_j + \beta_{ij}H_j \\ B_i &= h_{i\beta}\varepsilon_\beta + \beta_{ij}E_j + \gamma_{ij}H_j \end{aligned} \tag{63}$$

where the subscripts $\alpha, \beta = 1, 2, ..., 6$ and $i, j = 1, 2, 3$. The material constants in all examples are expressed in Voigt notation and four types of material constants shown in Table 1 are used in this paper which are denoted by (a) PE: the properties of PE phase ($BaTiO_3$) used in Examples 6 and 7; (b) PM: the properties of PM phase ($CoFe_2O_4$) used in Examples 6 and 7; (c) MEE1: the effective homogenized properties of the $BaTiO_3$-$CoFe_2O_4$ particulate composite with the particle volume fraction $V_f = 0.5$ used in Examples 1, 2, 3, 6 and 7; (d) MEE2: the properties of the homogeneous MEE material used in Examples 4 and 5. The poling directions in all examples are all assumed to be along x_2-axis in this paper.

7.1 Fracture of homogeneous MEE materials

Example 1: Central straight crack in a 2D MEE plate

As shown in Fig. 6(a), the first example is a center-cracked homogeneous MEE plate of length $4W$ and width $2W$ subjected to far-field tensile stress σ_0, electric displacement D_0 and magnetic induction B_0 on the remote boundary. The plate contains a horizontal crack of length $2a$ with the center coinciding with the origin. The data used in the analysis are as follows: $W = 1$; $a/W = 0.2$; $\sigma_0 = 1\ \text{N/m}^2$; $D_0 = 10^{-9}\ \text{C/m}^2$; $B_0 = 10^{-8}\ \text{N/Am}$. The material is taken to be $BaTiO_3$-$CoFe_2O_4$ composite with a volume fraction $V_f = 0.5$, and the material constants are given in Table 1 (see MEE1).

Fig. 6(b) shows the mesh configuration. Eight-node quadrilateral (Q8) elements are

used over most of the mesh and six-node quarter-point (T6qp) singular elements are employed around the crack tips to improve the accuracy for the stress, electric displacement and magnetic induction fields exhibit an inverse square root singularity. The mesh consists of 1970 regular Q8 elements, 22 T6qp elements around the crack tips and 45 enriched elements containing the crack face, with a total of 2037 elements and 6238 nodes.

In order to determine the integral domain, as shown in Fig. 7, we first built a referenced circular contour C_I of radius R_I, and the elements cut by C_I and surrounded by C_I constitute the integral domain. In order to verify the convergence of the IFs, 10 integral domains of different size are adopted, namely, $R_I/h_e = 1 \sim 512$, where h_e denotes the radial-edge length of the crack-tip element. In this example, $h_e = 3.03\times10^{-4}$.

In all examples, we define the normalized SIFs as $K_I^* = K_I/K^0$ and $K_{II}^* = K_{II}/K^0$, the normalized EDIF as $K_D^* = K_D/K_D^0$ and the normalized MIIF as $K_B^* = K_B/K_B^0$, where K^0, K_D^0 and K_B^0 are the normalized factors. In Example 1, the normalized factors $K^0 = \sigma_0\sqrt{\pi a}$, $K_D^0 = D_0\sqrt{\pi a}$ and $K_B^0 = B_0\sqrt{\pi a}$. Table 2 lists the normalized IFs obtained at the right crack tip. The results show that each of the IFs converges to a stable value when the integral domain reaches an enough size, such as $R_I/h_e \geq 4$ for this example. In comparison of the present results for $R_I/h_e \geq 4$ and those given by Rojas-Diaz et al. (2012), the relative errors of K_I^*, K_D^* and K_B^* are respectively within 0.2%, 0.2% and 0.3%.

Example 2: Three parallel cracks in an infinite 2D MEE solid

As shown in Fig. 8, another model is a homogeneous MEE plate with three parallel cracks $C1$, $C2$ and $C3$. The problem of an infinite plate with such a configuration was investigated by Rojas-Diaz et al. (2012). In order to simulate an infinite solid, the plate length $2W$ remains fixed at 20 times of the crack length $2a$. The data used in the analysis are as follows: $a=1$; $W=20$; $\sigma_0=1$ N/m^2; $D_0=10^{-9}$ C/m^2; $B_0=10^{-8}$ N/Am. The material constants of MEE1 in Table 1 are also adopted in this example.

The mesh consists of 2039 elements and 6060 nodes. Here, $h_e=2.01\times10^{-3}$ and $R_I/h_e=4$ which leads to that the integral domain contains four layer elements around the crack tips as shown in Fig. 7. The normalized factors are taken to be $K^0=\sigma_0\sqrt{\pi a}$, $K_D^0=D_0\sqrt{\pi a}$ and $K_B^0=B_0\sqrt{\pi a}$, and Table 3 lists the normalized IFs at the right tip of the cracks $C1$ and $C2$. The relative errors between present results and those given by Rojas-Diaz et al. (2012) are all within 3.0%.

Example 3: a circular arch crack in an infinite 2D MEE solid

To further confirm the validity of the interaction integral for a curved crack, as shown in Fig. 9, a circular arch crack in a 2D MEE plate is considered. The problem of an infinite solid with such a configuration was investigated by Garcia-Sanchez et al. (2007) and Feng et al. (2011). The radius and central angle of the crack are r_0 and θ, respectively and take $r_0/W=0.1$ to simulate an infinite solid. The data used in the analysis are as follows: $r_0=1$; $\theta=15°\sim75°$; $W=10$. Table 1 lists the material constants (see MEE1). In this example, the following two loading cases are considered:

Case 1: the pure mechanical loading, i.e., $\sigma_0=1$ and $D_0=B_0=0$;

Case 2: the magneto-electro-mechanical loading, i.e., $\sigma_0 = 1$, $D_0 = \lambda_D \sigma_0$ and $B_0 = \lambda_B \sigma_0$, where the parameters $\lambda_D = e_{33}/C_{33}$ and $\lambda_B = h_{33}/C_{33}$.

The normalized factors are taken to be $K^0 = \sigma_0 \sqrt{\pi r_0 \sin\theta}$, $K_D^0 = \lambda_D \sigma_0 \sqrt{\pi r_0 \sin\theta}$ and $K_B^0 = \lambda_B \sigma_0 \sqrt{\pi r_0 \sin\theta}$ for both the above cases.

For Case 1, the mesh consists of 1469 elements and 4454 nodes. Here, $h_e = 1.17 \times 10^{-3}$ and $R_I / h_e = 4$. Table 4 lists the normalized IFs obtained here and those in published articles. It can be observed that compared with the other SIFs in Table 4, the value of K_I^* for $\theta = 75°$ is very small. And except it, the relative errors of K_I^* and K_{II}^* between present results and those in published papers (Garcia-Sanchez et al., 2007; Feng et al., 2011) are all within 3.5%.

For Case 2, the mesh consists of 1661 elements and 5030 nodes. Here, $h_e = 5.14 \times 10^{-4}$. As shown in Fig. 10, six integral domains of different size ($R_I / h_e = 4 \sim 128$) are selected to check the variations of the IFs. In order to estimate the deviation of the IFs, the relative error is defined as

$$E_{rr} = \left| \frac{K_{\max} - K_{\min}}{K_{\text{mean}}} \right| \times 100\% \tag{64}$$

where $K_{\max}$, $K_{\min}$ and K_{mean} denote the maximum, minimum and mean of the IFs, respectively, obtained by different integral domains. Table 5 lists the normalized IFs and the corresponding relative errors E_{rr}. The relative errors E_{rr} are all within 1.0%, which demonstrates the domain-independence of the interaction integral. It should be pointed out that the term $I_{crackface}$ in Eq. (58) is not considered in the computation of the interaction integral. It can be observed from Table 5 that the contribution of the term $I_{crackface}$ is not obvious for $R_I / h_e \le 128$ (or $R_I / 2\pi r_0 \le 1.0\%$) in this example.

7.2 Fracture of non-homogeneous MEE materials

Example 4: a horizontal crack in an infinite 2D FGMEE plate

Next, as shown in Fig. 11, a cracked FGMEE plate under remote loading is considered. The same problem was investigated by Rao and Kuna (2008b). The plate length $2W$ is ten times the larger of the crack length $2a$ for an approximation of an infinite plate. The material parameters are assumed to vary with x_1 according to

$$\begin{aligned}&(C_{\alpha\beta}, e_{i\beta}, h_{i\beta}, \kappa_{il}, \beta_{il}, \gamma_{il})\\&= (C_{\alpha\beta 0}, e_{i\beta 0}, h_{i\beta 0}, \kappa_{il0}, \beta_{il0}, \gamma_{il0})\,\mathrm{e}^{\zeta x_1}\end{aligned} \tag{65}$$

where $C_{\alpha\beta 0}$, $e_{i\beta 0}$, $h_{i\beta 0}$, κ_{il0}, β_{il0} and γ_{il0} are taken to be the material constants of MEE2 as shown in Table 1. The data used in the analysis are: $W=10$; $a=1$; $\zeta=-0.5\sim 0.5$; $\sigma_0=1$; $D_0=10^{-8}\sigma_0$; $B_0=\pm 10^{-6}\sigma_0$. The normalized factors are $K^0=\sigma_0\sqrt{\pi a}$, $K_D^0=10^{-8}\sigma_0\sqrt{\pi a}$ and $K_B^0=10^{-6}\sigma_0\sqrt{\pi a}$.

The mesh consists of 1185 elements and 3570 nodes. Here, $h_e=1.54\times 10^{-3}$ and $R_I/h_e=4$. Fig. 12 presents the normalized IFs of the right crack tip. The relative errors of K_I^*, K_D^* and K_B^* between the present values and those given by Rao and Kuna (2008b) are all within 2.4%, 3.5% and 0.7%, respectively.

Example 5: an inclined crack in a plate with four types of MEE properties

In order to check the domain-independence of the interaction integral for material non-homogeneity and discontinuity, as shown in Fig. 13(a), we select a MEE plate whose properties vary with x_1 according to

$$\begin{aligned}&(C_{\alpha\beta}, e_{i\beta}, h_{i\beta}, \kappa_{il}, \beta_{il}, \gamma_{il})\\&= (C_{\alpha\beta 0}, e_{i\beta 0}, h_{i\beta 0}, \kappa_{il0}, \beta_{il0}, \gamma_{il0})\times f(x_1)\end{aligned} \tag{66}$$

where $C_{\alpha\beta 0}$, $e_{i\beta 0}$, $h_{i\beta 0}$, κ_{il0}, β_{il0} and γ_{il0} are the material constants of MEE2 as

shown in Table 1. As shown in Fig. 14, four functions used in this example are :

1) constant, $f(x_1)=1$;

2) linear, $f(x_1)=1+x_1/2W$;

3) exponential, $f(x_1)=\mathrm{e}^{x_1/2W}$;

4) jump, $f(x_1)=\begin{cases}1 & (x_1\le 0)\\ 2 & (x_1>0)\end{cases}$.

The constant function denotes a homogeneous MEE material, the linear and exponential functions denote two FGMEE materials, and the jump function denotes a discontinuous MEE material with a vertical interface at $x_1=0$. Correspondingly, the domain-independence of the interaction integral will be verified for homogeneous, non-homogeneous and discontinuous MEE materials successively. The plate of length $2L$ and width $2W$ contains an inclined crack AB of length $2a$ which occupies the segment from $A(-4.6,-1)$ to $B(-0.6,1)$. The following data are used for numerical analysis: $L=30$; $W=10$; $\sigma_0=1$; $D_0=10^{-10}\sigma_0$; $B_0=10^{-8}\sigma_0$. The normalized factors are $K^0=\sigma_0\sqrt{\pi a}$, $K_D^0=D_0\sqrt{\pi a}$ and $K_B^0=B_0\sqrt{\pi a}$.

Fig. 13(b) shows the corresponding mesh configuration consisting of 1982 elements and 6069 nodes. Here, $h_e=1.02\times10^{-2}$ and eight integral domains ($R_I/h_e=3\sim3\times2^7$) are selected to check the variations of the IFs. As shown in Figs. 15(a) and (b), for the jump function, the domains $R_I/h_e=3\sim3\times2^4$ do not contain the vertical interface while the domains $R_I/h_e=3\times2^5\sim3\times2^7$ contain it. Table 6 lists the normalized IFs and the corresponding relative errors E_{rr}. It can be observed that the relative errors of all IFs are within 0.20% for every function $f(x_1)$, which implies the interaction integral is domain-independent for material non-homogeneity and discontinuity.

Example 6: a crack in a particulate MEE plate

In order to verify the domain-independence of the interaction integral for curved interfaces, a $BaTiO_3$-$CoFe_2O_4$ particulate MEE plate is considered. As shown in Fig. 16, the square plate of unit length contains an inclined crack of length $2a$ and angle θ measured counterclockwise. 16 circular $CoFe_2O_4$ particles of radius r_0 are uniformly distributed in the $BaTiO_3$ matrix and thus, the plate is composed of 16 square cells of length $W/2$ each of which contains a circular particle of radius r_0 at its center. The volume fraction of the particles is $V_f = 4\pi r_0^2 / W^2$. The poling directions of the matrix and the particles are all assumed to be along x_2-axis. The corresponding material constants are given in Table 1 and the other data used in the analysis are: $W = 0.5$; $V_f = 0.5$; $\theta = (0°, 36°)$; $\sigma_0 = 1$; $D_0 = 10^{-10}\sigma_0$; $B_0 = 10^{-8}\sigma_0$. The normalized factors are $K^0 = \sigma_0\sqrt{\pi a}$, $K_D^0 = D_0\sqrt{\pi a}$ and $K_B^0 = B_0\sqrt{\pi a}$.

Figs. 17(a) and (b) show the mesh configurations corresponding to $\theta = 0°$ and $\theta = 36°$, respectively, each of which consists of 1009 elements and 3082 nodes. Here, $h_e = 0.63\times10^{-3}$ and eight integral domains $R_I/h_e = 3 \sim 3\times2^7$ are also adopted to check the variations of the IFs. The domains $R_I/h_e = 3 \sim 3\times2^4$ do not contain interfaces while the domains $R_I/h_e = 3\times2^5 \sim 3\times2^7$ contain interfaces. Table 7 lists the normalized IFs and the corresponding relative errors E_{rr}. The relative errors of the IFs are all within 0.8%. From this example, it can be seen that the interaction integral may become a very promising technique in the fracture analysis of MEE materials with complex interfaces.

Meanwhile, an equivalent homogeneous MEE plate of the same geometry and

boundary conditions as shown in Fig. 16 is adopted to compare the IFs. The material properties are taken to be the homogenized effective properties of $CoFe_2O_4$-$BaTiO_3$ composite with $V_f = 0.5$ shown in Table 1 (see MEE1). The normalized IFs are listed in Table 8 in which the symbols "PE-PM" and "MEE1" denote the $CoFe_2O_4$-$BaTiO_3$ particulate plate and the equivalent homogenous MEE plate, respectively. The differences of the IFs between the particulate plate and the equivalent homogeneous plate imply that in a certain scale, we may not obtain an expected result by applying the homogenized effective properties in the fracture analysis of actual particulate MEE composites.

7.3 Fracture of particulate MEE composites

The accuracy and domain-independence of the interaction integral have been verified in Sections 7.1 and 7.2, good results imply that the interaction integral is of effectiveness in linear fracture analyses of MEE materials with complex interfaces. Besides, the differences of the IFs between a particulate MEE plate and an equivalent homogeneous MEE plate have been observed and hence, a further study on a particulate MEE plate with an edge crack will be given in this section.

Example 7: an edge crack in a particulate MEE plate

Fig. 18 shows a particulate MEE plate of width $W = 1$ and length $3W = 3$ which contains an edge crack of length a at the center of the plate. The plate contains 40 elliptical particles of same size which are distributed randomly throughout the matrix with a total volume fraction $V_f = 0.5$. The crack length a is taken to be $0.36W$ and $0.5W$, respectively, to study the distinction of the IFs for the crack tip located in

different phases. In details, as shown in Fig. 18, the crack tip lies in a particle for $a = 0.36W$ and in the matrix for $a = 0.5W$.

Four computational schemes of different level in homogenizing the material properties will be adopted in this example. Before introducing these schemes, we first plot a rectangular box of $2w_{enr} \times 2w_{enr}$ with the center at the crack tip, as shown in Fig. 19(b) and (c), and then, name the area in the rectangular box as the near-tip region and the remaining area as the far-tip region. In this example, $w_{enr} = 0.2W$. These schemes can be described as follows:

Scheme 1: the enrichment corresponding to the interface ($\psi(\mathbf{x})b_I^P$ in Eq. (61)) is added into the approximations of the expanded displacements for all particles. Therefore, all particles can be called as the "enriched particles" whose boundaries are marked by black solid lines in Fig. 19(a).

Scheme 2: the enrichment corresponding to the interface is added only for the particles totally and partially in the near-tip region. As shown in Fig. 19(b), four particles are selected to be the "enriched particles". Moreover, although the nodal displacements for most of elements in Scheme 2 are not enriched by the term $\psi(\mathbf{x})b_I^P$, as shown in Fig. 20, the distribution of the integral points and the properties at the integral points used in Scheme 1 are the same as those used in Scheme 2.

Scheme 3: as shown in Fig. 19(c), actual properties of PE phase and PM phase are adopted for the elements totally and partially in the near-tip region, and the homogenized effective properties (MEE1 in Table 1) are used for the

remaining elements.

Scheme 4: as shown in Fig. 19(d), the homogenized effective properties are used for all elements.

It can be observed that the property-homogenization level increases from Scheme 1 to Scheme 4. In details, compared with Scheme 1, Scheme 2 ignores the influences of the interfaces far away from the crack tip. Compared with Scheme 2, Scheme 3 replaces the actual properties by the homogenized effective properties in the region far away from the crack tip. Compared with Scheme 3, Scheme 4 replaces the actual properties by the homogenized effective properties for the whole plate.

At first, the pure mechanical loading, $\sigma_0 = 1$ and $D_0 = B_0 = 0$, is applied along the top and bottom edges. Here, the matrix and the particles are taken to be $BaTiO_3$ and $CoFe_2O_4$, respectively. The normalized factors are taken to be $K^0 = \sigma_0\sqrt{\pi a}$, $K_D^0 = 10^{-10}\sigma_0\sqrt{\pi a}$ and $K_B^0 = 10^{-8}\sigma_0\sqrt{\pi a}$ in this example, and the normalized IFs are listed in Table 9. It can be found that the IFs obtained by Scheme 2 are most close to those obtained by Scheme 1, and especially, the approximately same values of K_I^*, K_{II}^* and K_D^* are obtained by these two schemes. The differences of the IFs obtained by Scheme 1 and Scheme 3 are not obvious for $a = 0.36W$, but become prominent for $a = 0.5W$. And the IFs obtained by Scheme 4 are distinctly different from those obtained by Scheme 1. The results imply that in the fracture analysis of a particulate MEE material under pure mechanical loading, Schemes 3 and 4 could not solve the IFs effectively while Scheme 2 may be used as a simplified approach to replace Scheme 1.

Next, the magneto-electro-mechanical loading, $\sigma_0 = 1$, $D_0 = 10^{-10}\sigma_0$ and

$B_0 = 10^{-8}\sigma_0$, is applied. In order to study the effects of the matrix properties on the IFs, two constitutions of the particulate MEE plate are considered: (a) PE-matrix: $CoFe_2O_4$-particles distributed in the $BaTiO_3$-matrix; (b) PM-matrix: $BaTiO_3$-particles distributed in the $CoFe_2O_4$-matrix. Fig. 21(a) and (b) show the normalized IFs obtained using the above four schemes. It can be seen that the relative errors of the IFs for different schemes become a bit more obvious compared with pure mechanical loading. Especially, in comparison of Scheme 1 and Scheme 2, it can be observed that for both $a = 0.36W$ and $a = 0.5W$, the difference of K_B^* is largest for the PE-matrix plate, and in contrast, the difference of K_D^* is largest for the PM-matrix plate. It implies that for a particulate MEE composite, the PE-matrix composite is more sensitive to the property-homogenization level under the magnetic loading and in contrast, the PM-matrix composite is more sensitive under the electric loading. The reason may be that the matrix is connected as a whole while the particles are independently distributed. If the particles in the MEE composite can also form a skeleton, this phenomenon may disappear.

8. Summary and conclusions

This paper first introduces an expanded tensor notation to simplify the expressions of the basic equations of the MEE materials. Then, based on the expanded tensor notation, a domain-form interaction integral is derived for the computation of the intensity factors (IFs) of linear MEE materials. The present formulation does not contain any derivatives of material parameters. Moreover, it is proved that the interaction integral is still valid when the integral domain contains an arbitrary interface

and the interface does not affect its value. Namely, the interaction integral is domain-independent for material interfaces, which leads to that the interaction integral may become one of the most promising methods in linear fracture analyses of MEE materials with complex interfaces. By solving several benchmark fracture problems, excellent agreements are obtained in comparison of the present results and those in published articles, and the interaction integral exhibits good domain-independence for material non-homogeneity and discontinuity. Finally, four computational schemes of different property-homogenization level are adopted to study the particulate MEE plate. The results show that generally, the acceptable results can not be obtained by totally or partially using the homogenized effective properties to replace the actual PE and PM properties.

Acknowledgements

This work is sponsored by NSFC (Grant Nos. 11072068 and 11202058), the China Postdoctoral Science Foundation (Grant Nos. 20110491071 and 2012T50338), the Fundamental Research Funds for the Central Universities (Grant No. HIT. NSRIF. 2013082) and the Program of Excellent Team in Harbin Institute of Technology.

Appendix

In the local polar coordinate system shown in Fig. 1, the angular functions $f_J^N(\theta)$ and $g_{IJ}^N(\theta)$ can be obtained by means of the extended stroh formalism and semi-analytical calculations. Only 2D problems are focused in this paper. Therefore, $K_{III}=0$, $K_{III}^{aux}=0$ and the subscript $I,J=1,2,4,5$. Since $\sigma_{44}^{aux}=\sigma_{55}^{aux}=\sigma_{45}^{aux}=0$, only g_{I1}^N and g_{I2}^N are given due to the symmetry of the expanded auxiliary stress tensor.

The angular functions are expressed in terms of complex material eigenvalues P_α, eigenvectors $A_{M\alpha}$, and matrices $M_{M\alpha}$ and $N_{\alpha N}$ (Rao and Kuna, 2008b)

$$f_J^N = \sum_{\alpha=1}^{5} \mathrm{Re}\left\{ A_{J\alpha} N_{\alpha N} \sqrt{\cos\theta + p_\alpha \sin\theta} \right\} \tag{A1}$$

$$g_{I1}^N = -\sum_{\alpha=1}^{5} \mathrm{Re}\left\{ \frac{M_{I\alpha} N_{\alpha N} p_\alpha}{\sqrt{\cos\theta + p_\alpha \sin\theta}} \right\}, \qquad g_{I2}^N = \sum_{\alpha=1}^{5} \mathrm{Re}\left\{ \frac{M_{I\alpha} N_{\alpha N}}{\sqrt{\cos\theta + p_\alpha \sin\theta}} \right\} \tag{A2}$$

Here, Re{*} and Im{*} denote the real and imaginary parts, respectively, of the quantity in brackets. The five conjugate pairs of eigenvalues p_α, the (5×5) matrix of eigenvectors $A_{M\alpha}$ can be obtained by solving the following quadratic, eigenvalue problem:

$$\left[\mathbf{Q} + (\mathbf{R} + \mathbf{R}^T) p_\alpha + \mathbf{T} p_\alpha^2 \right] \mathbf{A}_\alpha = \mathbf{0} \tag{A3}$$

where $\mathbf{A}_\alpha = [A_{II\alpha} \quad A_{I\alpha} \quad A_{III\alpha} \quad A_{D\alpha} \quad A_{B\alpha}]^T$ and

$$\mathbf{Q} = \left[C_{I1K1}^{tip} \right], \quad \mathbf{R} = \left[C_{I1K2}^{tip} \right], \quad \mathbf{T} = \left[C_{I2K2}^{tip} \right] \tag{A4}$$

where C_{IJKL}^{tip} is the expanded stiffness tensor evaluated at the crack tip location. Eq. (A3) can be converted into the following eigenrelations:

$$\begin{bmatrix} -\mathbf{T}^{-1}\mathbf{R}^T & \mathbf{T}^{-1} \\ \mathbf{R}\mathbf{T}^{-1}\mathbf{R}^T - \mathbf{Q} & -\mathbf{R}(\mathbf{T}^{-1})^T \end{bmatrix} \boldsymbol{\xi} = p\boldsymbol{\xi} \tag{A5}$$

where the eigenvector $\boldsymbol{\xi} = [\mathbf{A}_\alpha^T \quad \mathbf{B}_\alpha^T]^T$, $\mathbf{B}_\alpha = [B_{II\alpha}, \ B_{I\alpha}, \ B_{III\alpha}, \ B_{D\alpha}, \ B_{B\alpha}]^T$. $\mathbf{A}_\alpha$ and $\mathbf{B}_\alpha$ satisfy the following relation

$$\mathbf{B}_\alpha = (\mathbf{R}^T + p_\alpha \mathbf{T})\mathbf{A}_\alpha = -\frac{1}{p_\alpha}(\mathbf{Q} + p_\alpha \mathbf{R})\mathbf{A}_\alpha \tag{A6}$$

Only the five eigenvalues p_α having positive imaginary part and the corresponding eigenvectors are used in Eqs. (A1) and (A2). The (5×5) $M_{M\alpha}$ and $N_{\alpha N}$ are

calculated by

$$\mathbf{N}^{-1} = \mathbf{M} = \left[M_{I\alpha} \right] = \left[(C_{I2K1} + C_{I2K2} p_\alpha) A_{K\alpha} \right] \tag{A7}$$

It should be noted that the summation convention is valid only for K, not for α.

The Irwin matrix $\mathbf{Y}$ is defined as

$$\mathbf{Y} = [Y_{MN}] = -\sum_{\alpha=1}^{5} \mathrm{Im}\{A_{M\alpha} N_{\alpha N}\} \tag{A8}$$

It is necessary to pointed out that the subscripts $M, N = \{II,\ I,\ III,\ D,\ B\}$ of the symbols $A_{M\alpha}$, $M_{M\alpha}$ and $N_{\alpha N}$ denote the crack opening modes with the values corresponding to a general subscript $I = \{1,\ 2,\ 3,\ 4,\ 5\}$, respectively.

References

Belytschko, T., Black, T., 1999. Elastic crack growth in finite elements with minimal remeshing. Int. J. Numer. Methods Eng. 45, 601-620.

Bhargava, R.R., Sharma, K., 2012. Application of X-FEM to study two-unequal-collinear cracks in 2-D finite magnetoelectoelastic specimen. Comput. Mater. Sci. 60, 75-98.

Chen, W.Q., Lee, K.Y., Ding, H., 2004. General solution for transversely isotropic magneto-electro-thermo-elasticity and the potential theory method. Int. J. Eng. Sci. 42, 1361-1379.

Cannillo, V., Manfredini, T., Montorsi, M., Siligardi, C., Sola, A., 2006. Microstructure-based modeling and experimental investigation of crack propagation in glass-alumina functionally graded materials. J. Eur. Ceram. Soc. 26, 3067-3073.

Chen, X.H., 2009. Energy release rate and path-independent integral in dynamic fracture of magneto-electro-thermo-elastic solids. Int. J. Solids Struct. 46, 2706-2711.

Dong, C.Y., Lo, S.H., Antes, H., 2008. Fracture analysis in 2D magneto-electro-elastic media by the boundary element method. Comput. Mech. 41, 207-217.

Enderlein, M., Ricoeur, A., Kuna, M., 2005. Finite element techniques for dynamic crack analysis in piezoelectrics. Int. J. Fract. 134, 191-208.

Feng, W.J., Su, R.K.L., 2006. Dynamic internal crack problem of a functionally graded magneto-electro-elastic strip. Int. J. Solids Struct. 43, 5196-5216.

Fries, T.P., 2008. A corrected XFEM approximation without problems in blending elements. Int. J. Numer. Methods Eng. 75, 503-532.

Feng, W.J., Li, Y.S., Han, X., Xu, Z.H., 2011. Application of the extended traction boundary element-free method to the fracture of two-dimensional infinite magnetoelectroelastic solid. Sci. China-Phys. Mech. Astron. 54(6), 1141-1153.

Gao, C.F., Kessler, H., Balke, H., 2003. Crack problems in magnetoelectroelastic solids. Part I: exact solution of a crack. Int. J. Eng. Sci. 41, 969-981.

Gao, C.F., Tong, P., Zhang, T.Y., 2004. Fracture mechanics for a mode III crack in a magnetoelectroelastic solid. Int. J. Solids Struct. 41, 6613-6629.

Garcia-Sanchez, F., Rojas-Diaz, R., Saez, A., Zhang, Ch., 2007. Fracture of magnetoelectroelastic composite materials using boundary element method (BEM). Theor. Appl. Fract. Mech. 47, 192-204.

Guo, J.H., Lu, Z.X., 2010. Anti-plane analysis of multiple cracks originating from a circular hole in a magnetoelectroelastic solid. Int. J. Solids Struct. 47, 1847-1856.

Hu, K.Q., Li, G.Q., 2005. Electro-magneto-elastic analysis of a piezoelectromagnetic strip with a finite crack under longitudinal shear. Mech. Mater. 37, 925-934.

Liu, J.X., Liu, X.L., Zhao, Y.B., 2001. Green's functions for anisotropic magnetoelectroelastic solids with an elliptical cavity or a crack. Int. J. Eng. Sci. 39, 1405-1418.

Li, X.F., 2005. Dynamic analysis of a cracked magnetoelectroelastic medium under antiplane mechanical

and inplane electric and magnetic impacts. Int. J. Solids Struct. 42, 3185-3205.

Li, Y.D., Lee, K.Y., 2008. Anti-plane crack intersecting the interface in a bonded smart structure with graded magnetoelectroelastic properties. Theor. Appl. Fract. Mech. 50, 235-242.

Li, Y.S., Feng, W.J., Xu, Z.H., 2009. Fracture analysis of cracked 2D planar and axisymmetric problems of magneto-electro-elastic materials by the MLPG coupled with FEM. Comput. Meth. Appl. Mech. Eng. 198, 2347-2359.

Lee, J.M., Ma, C.C., 2010. Analytical solutions for an antiplane problem of two dissimilar functionally graded magnetoelectroelastic half-planes. Acta Mech. 212, 21-38.

Moran, B., Shih, C.F., 1987. Crack tip and associated domain integrals from momentum and energy balance. Eng. Fract. Mech. 27(6), 615-642.

Moës, N., Dolbow, J., Belytschko, T., 1999. A finite element method for crack growth without remeshing. Int. J. Numer. Methods Eng. 46, 131-150.

Ma, L., Li, J., Abdelmoula, R., Wu, L.Z., 2007. Mode III crack problem in a functionally graded magneto-electro-elastic strip. Int. J. Solids Struct. 44, 5518-5537.

Ma, L., Wu, L.Z., Feng, L.P., 2009. Surface crack problem for functionally graded magnetoelectroelastic coating-homogeneous elastic substrate system under anti-plane mechanical and in-plane electric and magnetic loading. Eng. Fract. Mech. 76, 269-285.

Ma, C.C., Lee, J.M., 2009. Theoretical analysis of in-plane problem in functionally graded nonhomogeneous magnetoelectroelastic bimaterials. Int. J. Solids Struct. 46, 4208-4220.

Ma, P., Feng, W.J., Su, R.K.L., 2012. An electrically impermeable and magnetically permeable interface crack with a contact zone in a magnetoelectroelastic bimaterial under uniform magnetoelectromechanical loads. Eur. J. Mech. A-Solids 32, 41-51.

Pasternak, L., 2012. Doubly periodic arrays of cracks and thin inhomogeneities in an infinite magnetoelectroelastic medium. Eng. Anal. Bound. Elem. 36, 799-811.

Rao, B.N., Kuna, M., 2008a. Interaction integrals for fracture analysis of functionally graded piezoelectric materials. Int. J. Solids Struct. 45, 5237-5257.

Rao, B.N., Kuna, M., 2008b. Interaction integrals for fracture analysis of functionally graded magnetoelectroelastic materials. Int. J. Fract. 153, 15-37.

Rojas-Diaz, R., Garcia-Sanchez, F., Saez, A., 2010. Analysis of cracked magnetoelectroelastic composites under time-harmonic loading. Int. J. Solids Struct. 47, 71-80.

Rangelov, T., Stoynov, Y., Dineva, P., 2011. Dynamic fracture behavior of functionally graded magnetoelectroelastic solids by BIEM. Int. J. Solids Struct. 48, 2987-2999.

Rojas-Diaz, R., Sukumar, N., Saez, A., Garcia-Sanchez, F., 2011. Fracture in magnetoelectroelastic materials using the extended finite element method. Int. J. Numer Methods Eng. 88, 1238-1259.

Rekik, M., El-Borgi, S., Ounaies, Z., 2012. An Embedded Mixed-Mode Crack in a Functionally Graded Magnetoelectroelastic Infinite Medium. Int. J. Solids Struct. 49, 835-845.

Rojas-Diaz, R., Garcia-Sanchez, F., Saez, A., 2012. Dual BEM analysis of different crack face boundary conditions in 2D magnetoelectroelastic solids. Eur. J. Mech. A-Solids 31, 152-162.

Stern, M., Becker, E.B., Dunham, R.S., 1976. A contour integral computation of mixed-mode stress intensity factors. Int. J. Fract. 12, 359-368.

Song, Z.F., Sih, G.C., 2003. Crack initiation behavior in a magnetoelectroelastic composite under in-plane deformation. Theor. Appl. Fract. Mech. 39, 189-207.

Sladek, J., Sladek, V., Solek, P., Pan, E., 2008. Fracture analysis of cracks in magneto-electro-elastic solids by the MLPG. Comput. Mech. 42, 697-714.

Sladek, J., Sladek, V., Solek, P., Zhang, Ch., 2010. Fracture analysis in continuously nonhomogeneous magneto-electro-elastic solids under a thermal load by the MLPG. Int. J. Solids Struct. 47, 1381-1391.

Sladek, J., Sladek, V., Solek, P., Zhang, Ch., Wunsche, M., 2011. An interaction integral method for computing fracture parameters in functionally graded magnetoelectroelastic composites. CMC-Comput. Mat. Contin. 23, 35-68.

Tian, W.Y., Rajapakse, R.K.N.D., 2005. Fracture analysis of magnetoelectroelastic solids by using path independent integrals. Int. J. Fract. 131, 311-335.

Van Suchtelen, J., 1972. Product properties: a new application of composite materials. Phillips Res. Rep. 27, 28-37.

Van Run, A.M.J.G., Terrell, D.R., Scholing, J.H., 1974. An in situ grown eutectic magnetoelectric composite material: Part 2 Physical properties. J. Mater. Sci. 9, 1710-1714.

Wu, T.L., Huang, J.H., 2000. Closed-form solutions for the magnetoelectric coupling coefficients in fibrous composites with piezoelectric and piezomagnetic phases. Int. J. Solids Struct. 37, 2981-3009.

Wang, B.L., Mai, Y.W., 2003. Crack tip field in piezoelectric/piezomagnetic media. Eur. J. Mech. A-Solids 22, 591-602.

Wang, B.L., Mai, Y.W., 2004. Fracture of piezoelectromagnetic materials. Mech. Res. Commun. 31, 65-73.

Wang, B.L., Mai, Y.W., 2007. Applicability of the crack-face electromagnetic boundary conditions for fracture of magnetoelectroelastic materials. Int. J. Solids Struct. 44, 387-398.

Wunsche, M., Saez, A., Garcia-Sanchez, F., Zhang, Ch., 2012. Transient dynamic crack analysis in linear magnetoelectroelastic solids by a hypersingular time-domain BEM. Eur. J. Mech. A-Solids 32, 118-130.

Yong, H.D., Zhou, Y.H., 2007. Transient response of a cracked magnetoelectroelastic strip under anti-plane impact. Int. J. Solids Struct. 44, 705-717.

Yu, H.J., Wu, L.Z., Guo, L.C., Du, S.Y., He, Q.L., 2009. Investigation of mixed-mode stress intensity factors for nonhomogeneous materials using an interaction integral method. Int. J. Solids Struct. 46, 3710-3724.

Yu, H.J., Wu, L.Z., Guo, L.C., He, Q.L., Du, S.Y., 2010a. Interaction integral method for the interfacial fracture problems of two nonhomogeneous materials. Mech. Mater. 42, 435-450.

Yu, H.J., Wu L.Z., Guo L.C., Wu H.P., Du S.Y., 2010b. An interaction integral method for 3D curved cracks in nonhomogeneous materials with complex interfaces. Int. J. Solids Struct. 47, 2178-2189

Yu, H.J., Wu, L.Z., Guo, L.C., Ma, J.W., Li, H., 2012. A domain-independent interaction integral for fracture analysis of nonhomogeneous piezoelectric materials. Int. J. Solids Struct. 49, 3301-3315.

Zhou, Z.G., Wang, B., 2004. Two parallel symmetry permeable cracks in functionally graded piezoelectric/piezomagnetic materials under anti-plane shear loading. Int. J. Solids Struct. 41, 4407-4422.

Zhou, Z.G., Wang, B., 2006 The scattering of the harmonic anti-plane shear stress waves by two collinear interface cracks between two dissimilar functionally graded piezoelectric/piezomagnetic material half-infinite planes dynamic loading. PI Mech. Eng. C-J. Mech. 220, 137-148.

Zhou, Z.G., Chen, Z.T., 2008. Basic solution of a Mode-I limited-permeable crack in functionally graded piezoelectric/piezomagnetic materials. Int. J. Solids Struct. 45, 2265-2296.

Zhang, P.W., 2011. Dynamic fracture of a rectangular limited-permeable crack in magneto-electro-elastic media under a time-harmonic elastic P-wave. Int. J. Solids Struct. 48, 553-566.

Zhong, X.C., 2011. Closed-form solutions for two collinear dielectric cracks in a magnetoelectroelastic

solid. Appl. Math. Model. 35, 2930-2944.

Zhong, X.C., Lee, K.Y., 2012. Dielectric crack problem for a magnetoelectroelastic strip with functionally graded properties. Arch. Appl. Mech. 82, 791-807.

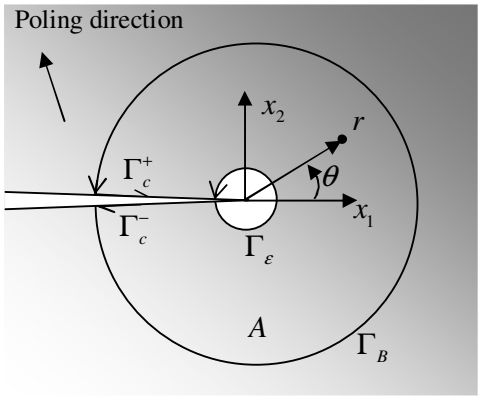

Fig. 1. Schematic illustration of some contour integrals and related equivalent domain integrals for a 2D cracked MEE solid.

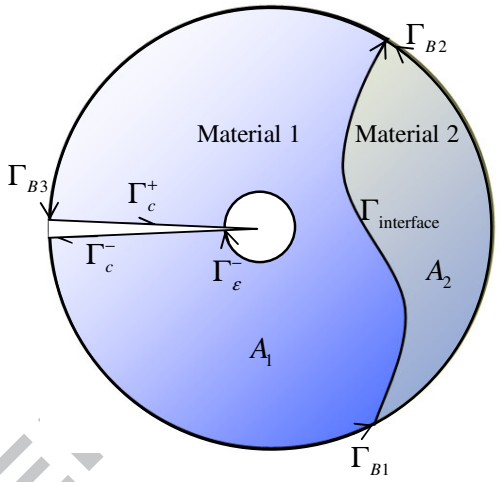

Fig. 2. An integral domain A divided by an interface $\Gamma_{\text{interface}}$ into two areas of different material properties A_1 and A_2.

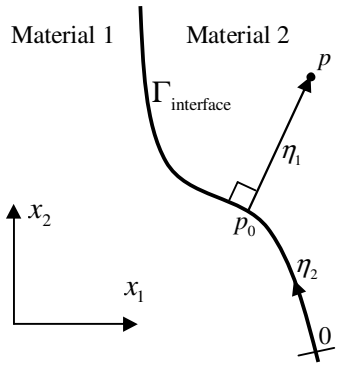

Fig. 3. A curvilinear coordinate system based on an interface.

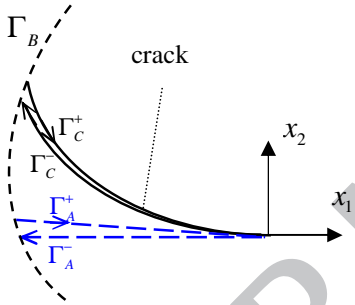

Fig. 4. Schematic illustration of a curved crack and a straight fictitious crack.

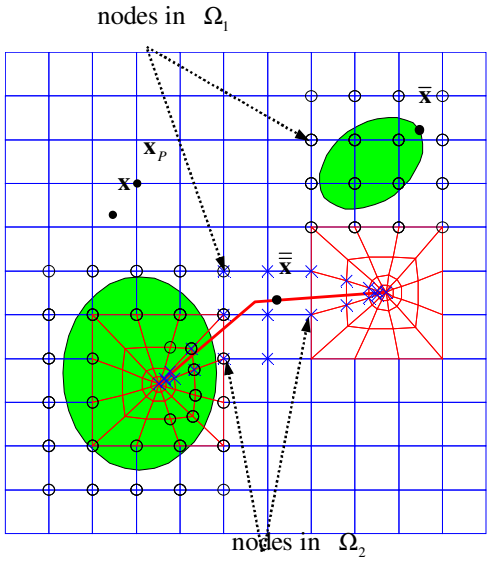

Fig. 5. Finite element mesh of a particulate MEE composite with a crack.

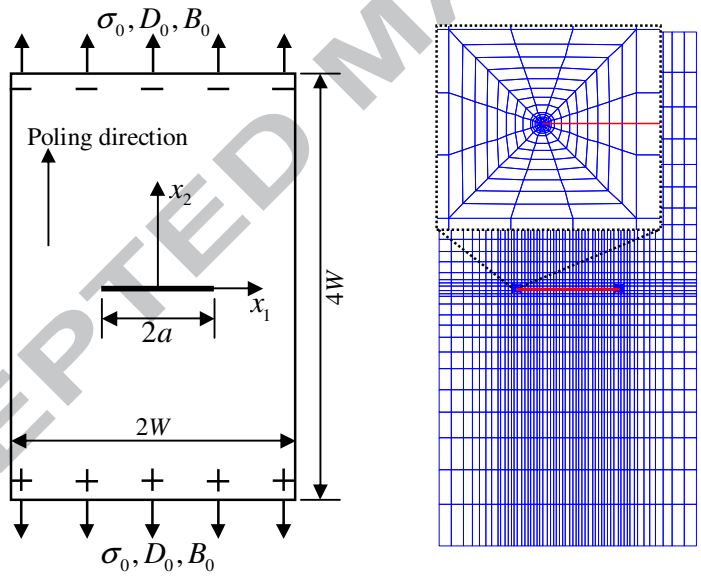

Fig. 6. A homogeneous MEE plate with a center crack: (a) geometry and boundary conditions; (b) finite element mesh.

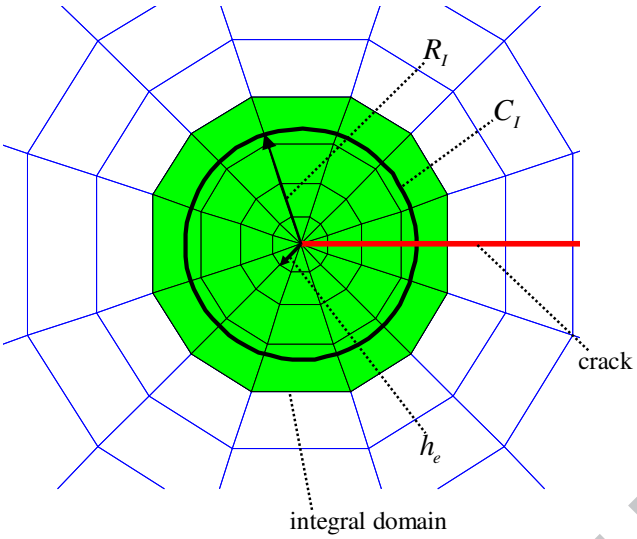

Fig. 7. An integral domain formed by the elements filled with green color.

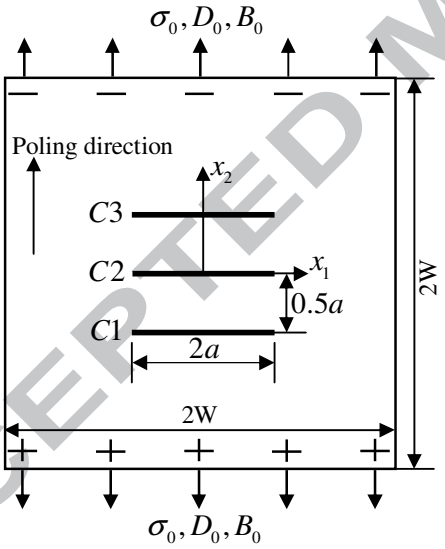

Fig. 8. A homogeneous MEE plate with three parallel cracks.

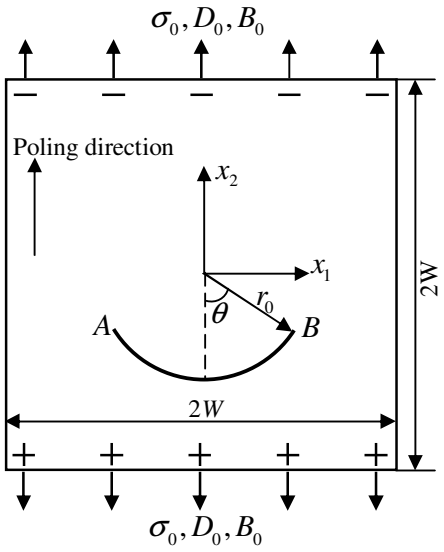

Fig. 9. A homogeneous MEE plate with a circular arch crack.

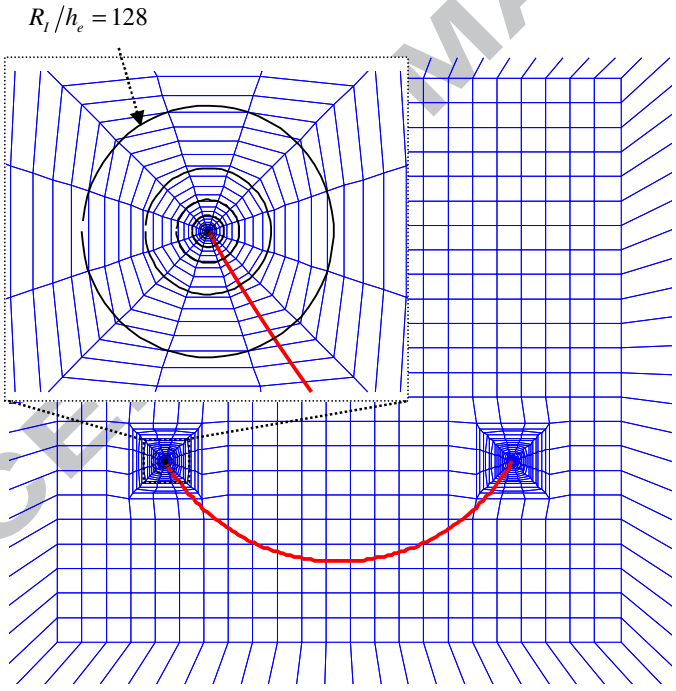

Fig. 10. Finite element mesh around the crack and reference circles C_I.

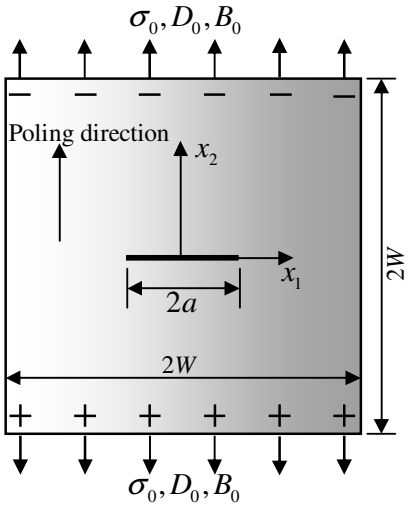

Fig. 11. A FGMEE plate with a horizontal crack.

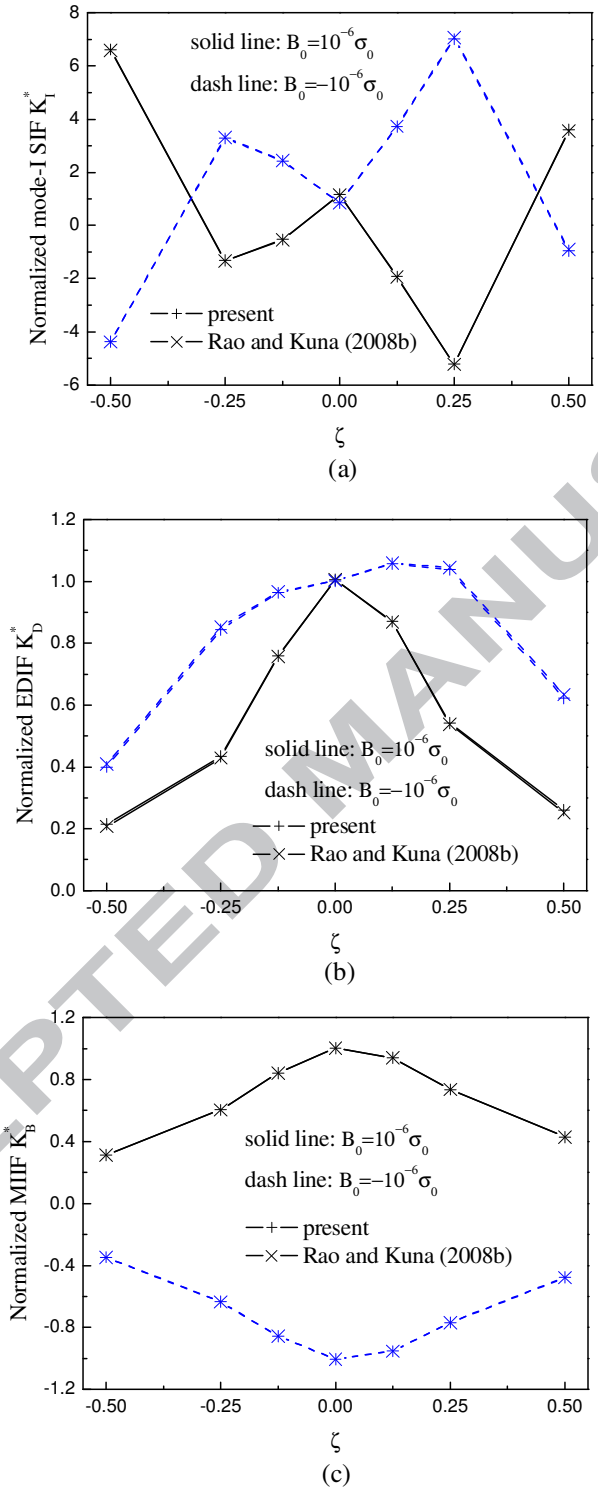

Fig. 12. Normalized IFs for a horizontal crack in a FGMEE plate: (a) K_I^* ; (b) K_D^* ; (c) K_B^* .

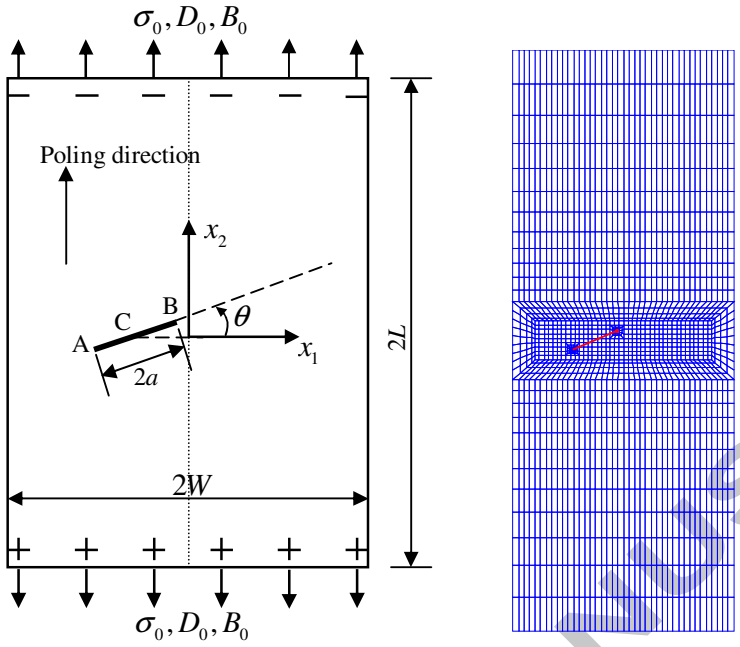

(a) (b)

Fig. 13. A MEE plate with an inclined crack AB: (a) geometry and boundary conditions; (b) finite element mesh.

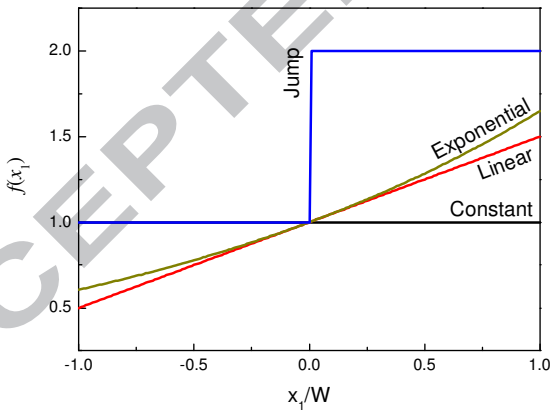

Fig. 14. Four types of material functions.

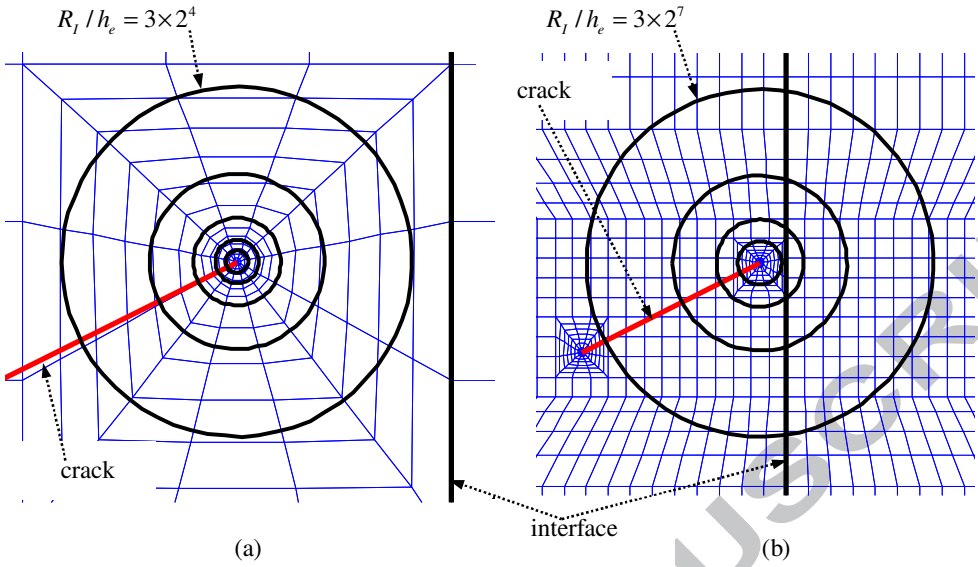

Fig. 15. Different integral domains surrounding the crack tip B: (a) $R_I / h_e = 3\times(1, 2, 2^2, 2^3, 2^4)$; (b) $R_I / h_e = 3\times(2^4, 2^5, 2^6, 2^7)$.

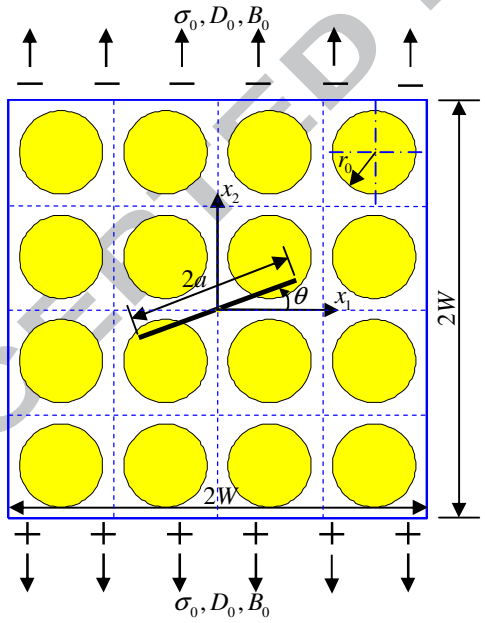

Fig. 16. A particulate MEE plate of unit length with an inclined center crack.

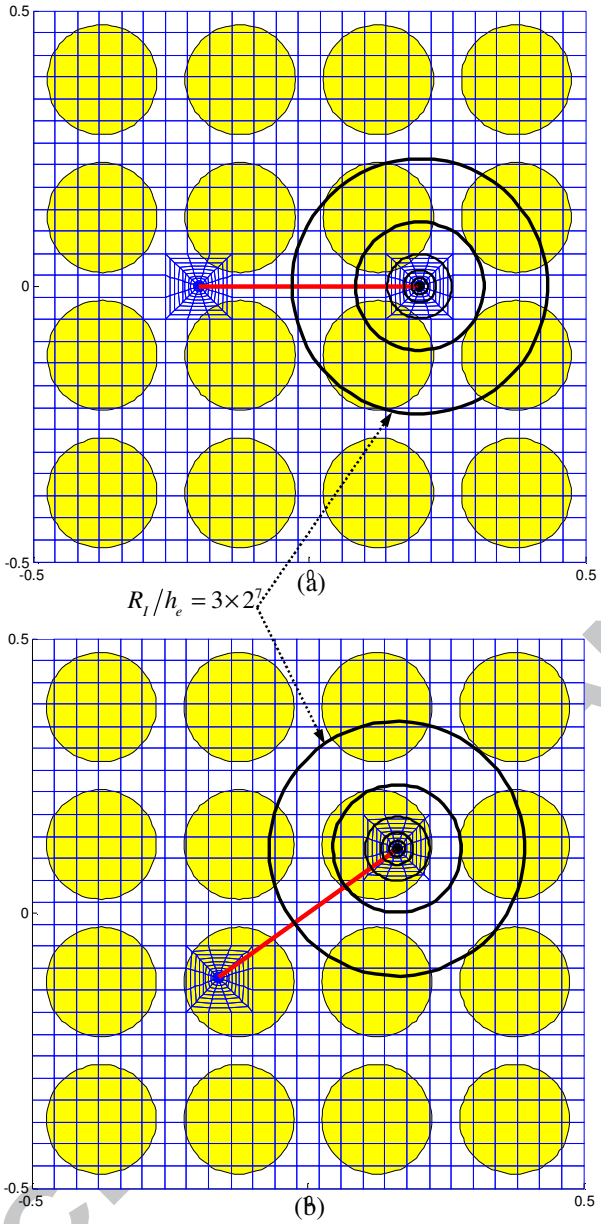

Fig. 17. Finite element mesh and integral domains of the particulate MEE plate with an inclined center crack: (a) $\theta = 0°$; (b) $\theta = 36°$.

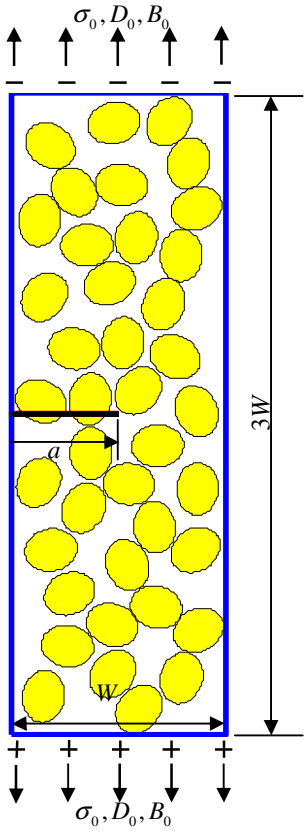

Fig. 18. A $BaTiO_3$-$CoFe_2O_4$ particulate plate with an edge crack.

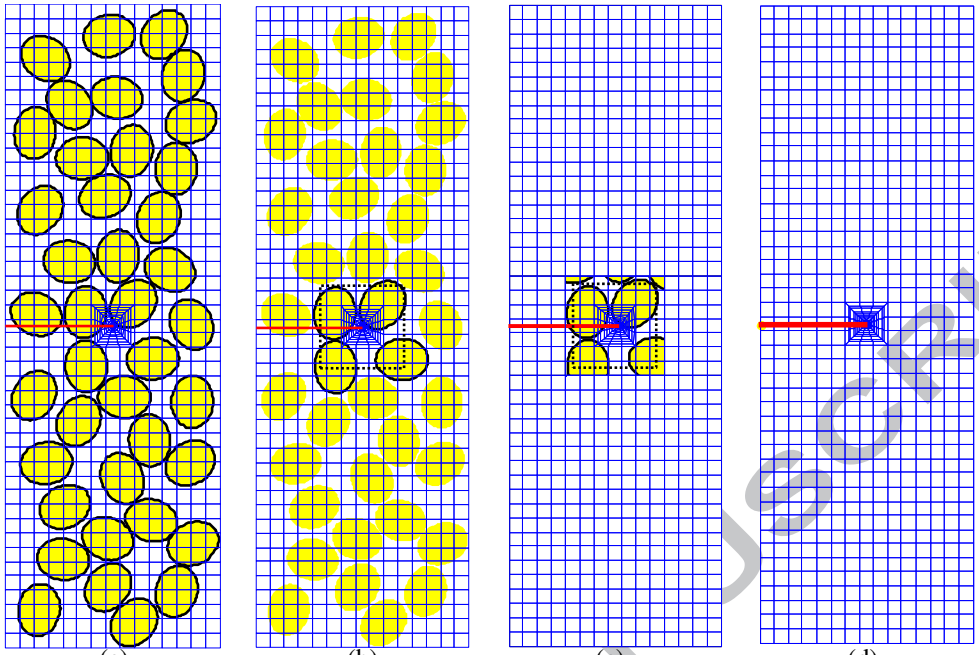

Fig. 19. Finite element mesh configurations for 4 computational schemes (the particles with the boundaries marked by black lines are the "enriched particles"): (a) Scheme 1; (b) Scheme 2; (c) Scheme 3; (d) Scheme 4.

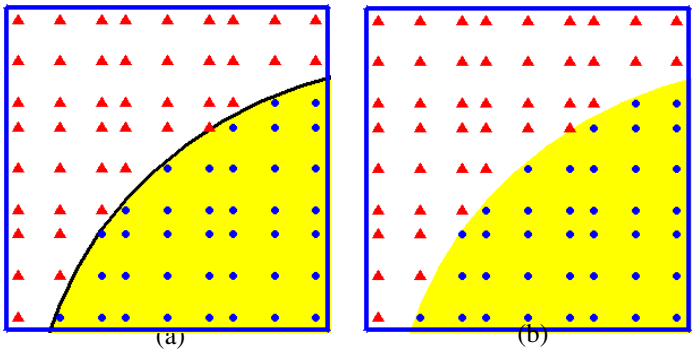

Fig. 20. Distribution of the integral points in an enriched element containing an interface (different shapes of the integral points denote different material constants): (a) for the nodal displacements enriched by $\psi(\mathbf{x})b_I^P$; (b) for the nodal displacements not enriched by $\psi(\mathbf{x})b_I^P$.

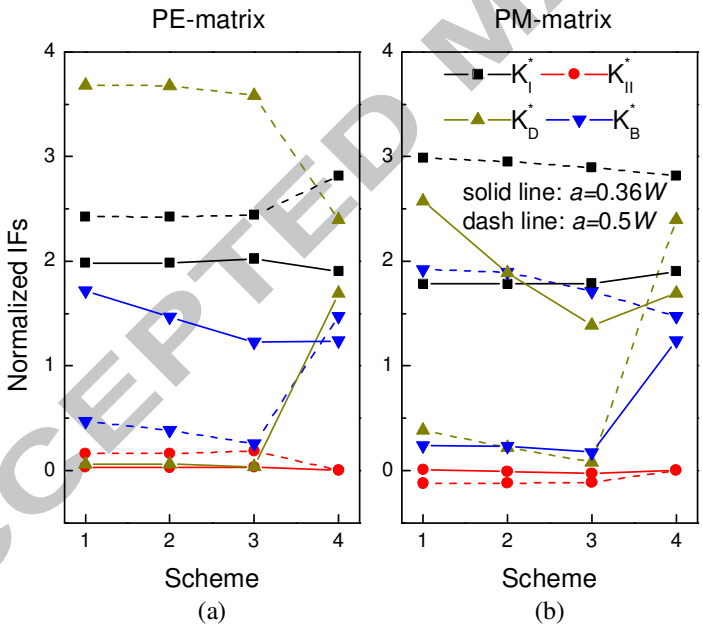

Fig. 21. Normalized IFs of different schemes for the plate under the magneto-electro-mechanical loading.

Table 1. Material constants.

Examples	6, 7		1, 2, 3, 6, 7	4, 5
Material constants	PE-PM (Pasternak, 2012)		MEE1: (Feng et al., 2011)	MEE2: (Rao and Kuna, 2008b)
	PE: $BaTiO_3$	PM: $CoFe_2O_4$	$BaTiO_3$-$CoFe_2O_4$ ($V_f = 0.5$)	
C_{11} (GPa)	166	286	226	166
C_{12} (Gpa)	77	173	125	77
C_{13} (Gpa)	78	170.5	124	78
C_{33} (Gpa)	162	269.5	216	162
C_{44} (Gpa)	43	45.3	44	43
e_{31} (C/m^2)	-4.4	0	-2.2	-4.4
e_{33} (C/m^2)	18.6	0	9.3	18.6
e_{15} (C/m^2)	11.6	0	5.8	11.6
h_{31} (N/Am)	0	580.3	290.2	580.3
h_{33} (N/Am)	0	699.7	350	699.7
h_{15} (N/Am)	0	550	275	550
κ_{11} (10^{-9}C^2/Nm^2)	11.2	0.08	5.64	11.2
κ_{33} (10^{-9}C^2/Nm^2)	12.6	0.093	6.35	12.6
β_{11} (10^{-12}Ns/VC)	0	0	5.367	5
β_{33} (10^{-12}Ns/VC)	0	0	2737.5	3
γ_{11} (10^{-6}Ns^2/C^2)	5	590	297	5
γ_{33} (10^{-6}Ns^2/C^2)	10	157	83.5	10

Table 2. Normalized IFs at the right tip of a center crack in a homogeneous MEE plate (Example 1).

Present R_1/h_e	K_I^*	K_{II}^*	K_D^*	K_B^*
1	1.0258	-6.689×10^{-4}	1.0204	1.0223
2	1.0272	5.767×10^{-5}	1.0185	1.0190
4	1.0242	-8.542×10^{-7}	1.0171	1.0175
8	1.0242	4.305×10^{-7}	1.0173	1.0179
16	1.0238	3.498×10^{-7}	1.0180	1.0189
32	1.0242	3.905×10^{-7}	1.0175	1.0185
64	1.0241	3.703×10^{-7}	1.0175	1.0188
128	1.0240	3.517×10^{-7}	1.0175	1.0190
256	1.0239	2.551×10^{-7}	1.0174	1.0188
512	1.0240	3.485×10^{-7}	1.0175	1.0190
Rojas-Diaz et al. (2012)	1.0255	2.4187×10^{-9}	1.0190	1.0205

Table 3. Normalized IFs at the right tips of the cracks $C1$ and $C2$ in an infinite 2D MEE solid (Example 2).

	Present		Rojas-Diaz et al. (2012)		Relative errors	
	$C1$	$C2$	$C1$	$C2$	$C1$ (%)	$C2$ (%)
K_I^*	0.6943	0.4773	0.6865	0.4634	1.14	3.00
K_{II}^*	0.1386	7.945×10^{-10}	0.1379	~0	0.51	—
K_D^*	0.7439	0.6053	0.7405	0.5992	0.46	1.02
K_B^*	0.7947	0.6679	0.7939	0.6643	0.10	0.54

Table 4. Normalized IFs at the tip B of a circular arch crack in an infinite 2D MEE solid (Example 3, Case 1).

$\theta(°)$	Present				Feng et al. (2011)		Garcia-Sanchez et al. (2007)	
	K_I^*	K_{II}^*	K_D^*	K_B^*	K_I^*	K_{II}^*	K_I^*	K_{II}^*
15	0.9403	0.2539	-0.0314	-0.0565	0.9518	0.2631	0.95	0.25
30	0.7778	0.4684	-0.1006	-0.1682	0.7860	0.4841	0.78	0.47
45	0.5406	0.6140	-0.1761	-0.2487	0.5497	0.6299	0.54	0.62
60	0.2797	0.6684	-0.2322	-0.2834	0.2856	0.6844	0.27	0.67
75	0.0264	0.6367	-0.2599	-0.2908	0.0342	0.6499	0.03	0.65

Table 5. Normalized IFs at the tip B of a circular arch crack for different integral domains (Example 3, Case 2).

R_I/h_e	K_I^*	K_{II}^*	K_D^*	K_B^*
$\theta = 30°$				
4	0.7785	0.4695	0.8643	0.8633
8	0.7785	0.4696	0.8645	0.8627
16	0.7784	0.4696	0.8650	0.8600
32	0.7784	0.4701	0.8648	0.8618
64	0.7785	0.4656	0.8655	0.8564
128	0.7786	0.4667	0.8679	0.8566
E_{rr} (%)	0.03	0.96	0.42	0.80
$\theta = 60°$				
4	0.2803	0.6703	0.6277	0.7349
8	0.2804	0.6704	0.6278	0.7344
16	0.2803	0.6704	0.6283	0.7324
32	0.2802	0.6702	0.6285	0.7321
64	0.2803	0.6699	0.6277	0.7321
128	0.2803	0.6692	0.6271	0.7303
E_{rr} (%)	0.07	0.18	0.22	0.63

Table 6. Normalized IFs at the tip B for different integral domains (Example 5).

R_I/h_e	K_I^*	K_{II}^*	K_D^*	K_B^*
Constant				
3	0.83560	0.40571	0.93853	0.92712
3×2	0.83510	0.40539	0.93806	0.92660
3×2^2	0.83417	0.40497	0.93716	0.92578
3×2^3	0.83498	0.40520	0.93828	0.92606
3×2^4	0.83493	0.40512	0.93799	0.92634
3×2^5	0.83504	0.40525	0.93835	0.92651
3×2^6	0.83508	0.40498	0.93819	0.92645
3×2^7	0.83505	0.40500	0.93816	0.92643
E_{rr} (%)	0.172	0.182	0.145	0.145
Linear				
3	0.94899	0.44184	1.14343	0.94232
3×2	0.94842	0.44149	1.14286	0.94176
3×2^2	0.94736	0.44104	1.14180	0.94091
3×2^3	0.94827	0.44124	1.14310	0.94114
3×2^4	0.94820	0.44119	1.14279	0.94147
3×2^5	0.94833	0.44131	1.14319	0.94165
3×2^6	0.94837	0.44104	1.14302	0.94160
3×2^7	0.94833	0.44105	1.14298	0.94158
E_{rr} (%)	0.172	0.182	0.142	0.149
Exponential				
3	0.89693	0.42013	1.07638	0.89717
3×2	0.89639	0.41979	1.07584	0.89664
3×2^2	0.89539	0.41936	1.07484	0.89583
3×2^3	0.89626	0.41956	1.07607	0.89605
3×2^4	0.89619	0.41951	1.07578	0.89636
3×2^5	0.89631	0.41963	1.07616	0.89653
3×2^6	0.89635	0.41936	1.07599	0.89648
3×2^7	0.89631	0.41938	1.07595	0.89646
E_{rr} (%)	0.172	0.182	0.142	0.149
Jump				
3	0.61449	0.28473	0.71671	0.61086
3×2	0.61412	0.28451	0.71635	0.61050
3×2^2	0.61343	0.28421	0.71568	0.60995
3×2^3	0.61403	0.28434	0.71650	0.61009
3×2^4	0.61394	0.28433	0.71624	0.61028
3×2^5	0.61405	0.28441	0.71659	0.61040
3×2^6	0.61409	0.28423	0.71646	0.61039
3×2^7	0.61406	0.28425	0.71643	0.61038
E_{rr} (%)	0.172	0.184	0.144	0.150

Table 7. Normalized IFs obtained by different integral domains at the right tip of a crack in a particulate MEE plate (Example 6).

R_I/h_e	K_I^*	K_{II}^*	K_D^*	K_B^*
$\theta=0°$				
3	1.18049	7.98×10^{-14}	1.63425	0.79944
3×2	1.18065	7.34×10^{-14}	1.63431	0.80022
3×2^2	1.18071	7.63×10^{-14}	1.63441	0.80063
3×2^3	1.18072	8.17×10^{-14}	1.63462	0.80088
3×2^4	1.18076	8.22×10^{-14}	1.63479	0.80103
3×2^5	1.18084	8.67×10^{-14}	1.63336	0.80103
3×2^6	1.18073	8.75×10^{-14}	1.63488	0.80005
3×2^7	1.18018	9.55×10^{-14}	1.63770	0.79871
E_{rr} (%)	0.05	--	0.26	0.29
$\theta=36°$				
3	0.88983	0.59665	0.015906	1.36522
3×2	0.88961	0.59755	0.015920	1.36688
3×2^2	0.88937	0.59797	0.015927	1.36783
3×2^3	0.88905	0.59816	0.015931	1.36846
3×2^4	0.88886	0.59828	0.015933	1.36898
3×2^5	0.88875	0.59839	0.015939	1.36956
3×2^6	0.88863	0.59832	0.015944	1.37255
3×2^7	0.88864	0.59842	0.015920	1.37516
E_{rr} (%)	0.13	0.30	0.24	0.72

Table 8. Normalized IFs at the right tip of a center crack in a particulate MEE plate (Example 6).

Types of the plate	K_I^*	K_{II}^*	K_D^*	K_B^*
$\theta=0°$				
PE-PM	1.1806	0	1.6348	0.8002
MEE1	1.2086	0	1.1710	1.0934
$\theta=36°$				
PE-PM	0.8891	0.5980	0.0159	1.3693
MEE1	0.7916	0.5481	0.9373	0.8959

Table 9. Normalized IFs obtained by different schemes for a particulate MEE plate under pure mechanical loading (Example 7, $\sigma_0 = 1$, $D_0 = B_0 = 0$).

Schemes	K_I^*	K_{II}^*	K_D^*	K_B^*
$a = 0.36W$				
Scheme1	1.9613	0.0290	-0.0038	0.2205
Scheme 2	1.9606	0.0290	-0.0038	0.2346
Scheme 3	1.9732	0.0296	-0.0036	0.2409
Scheme 4	1.9015	7.89×10^{-8}	0.6361	0.1839
$a = 0.5W$				
Scheme 1	2.5888	0.1498	1.7340	-0.0012
Scheme 2	2.5877	0.1502	1.7398	0.0014
Scheme 3	2.5672	0.1618	1.9641	0.0070
Scheme 4	2.8149	5.51×10^{-8}	1.2663	0.3476